Progress in Neurobiology 249 (2025) 102773

Contents lists available at ScienceDirect

Progress in Neurobiology

journal homepage: www.elsevier.com/locate/pneurobio

Glycine-gated extrasynaptic NMDARs activated during glutamate spillover drive burst firing in nigral dopamine neurons

Sofian Ringlet [a,c], Zoraide Motta [b], Laura Vandries [c], Vincent Seutin [c], Kevin Jehasse [d], Laura Caldinelli [b], Loredano Pollegioni [b], Dominique Engel [a,*,1]

[a] GIGA-Neurosciences, Laboratory of Molecular Regulation of Neurogenesis, University of Liege, Avenue Hippocrate 15, Liege B-4000, Belgium
[b] The Protein Factory 2.0 Lab, Dipartimento di Biotecnologie e Scienze della Vita, Università degli Studi dell'Insubria, via Dunant, Varese 3-21100, Italy
[c] GIGA-Neurosciences, Neurophysiology group, University of Liege, Avenue Hippocrate 15, Liege B-4000, Belgium
[d] Montefiore Institute of Electrical Engineering and Computer Science, Systems and Modeling research unit at University of Liège, Quartier Polytech 1, allée de la Découverte 10, Liège 4000, Belgium

ARTICLE INFO

Keywords:
Excitatory postsynaptic current
NMDA receptor
Burst | substantia nigra
Patch-clamp
D-serine
Glycine
Co-agonist

ABSTRACT

Burst firing in substantia nigra pars compacta dopamine neurons is a critical biomarker temporally associated to movement initiation. This phasic change is generated by the tonic activation of NMDARs but the respective role of synaptic versus extrasynaptic NMDARs in the ignition of a burst and what is their level of activation remains unknown. Using ex vivo electrophysiological recordings from adolescent rats, we demonstrate that extrasynaptic NMDARs are the primary driver of burst firing. This pool of receptors is recruited during intense synaptic activity via spillover of glutamate and require the binding of NMDAR co-agonist glycine for full activation. Basal synaptic transmission activating only synaptic NMDARs with the support of D-serine is insufficient to generate a burst. Notably, both synaptic and extrasynaptic NMDARs share the same subunit composition but are regulated by distinct co-agonists. Location of NMDARs and regionalization of co-agonists but not NMDAR subunit composition underly burst generation and may serve as a guideline in understanding the physiological role of dopamine in signaling movement.

1. Introduction

Activity of dopamine (DA) neurons in the substantia nigra pars compacta (SNc) provides essential signal to the dorsal striatum for the control of movement (Howe and Dombeck, 2016; da Silva et al., 2018). The fragility of DA neurons located precisely in this brain region is at the origin of the severe motor deficits expressed in Parkinson's disease (PD) (Hornykiewicz, 2006). The fundamental function ensured by SNc DA neurons is encoded by transitions of their output signal from spontaneous low-frequency action potential (AP) firing to high-frequency bursts of APs (Grace and Bunney, 1984). Bursting is a key electrophysiological signal producing an increase of DA release in postsynaptic target areas (Gonon, 1988; Ammari et al., 2009), which is temporally correlated to locomotion initiation (Howe and Dombeck, 2016; da Silva et al., 2018). Ignition of a burst is operated by N-methyl-D-aspartate receptors (NMDARs) activated by synaptic glutamate released from excitatory afferents (Chergui et al., 1994) originating predominantly from the subthalamic nucleus (STN), pedunculopontine nucleus (PPN) and cortex (Watabe-Uchida et al., 2012). While bursts critically depend on the presence of the GluN1 subunit (Wang et al., 2011; Zweifel et al., 2009), the link between the activation of NMDARs and the generation of a burst is not well understood. This lack of information is surprising since bursts mediate the increased dopamine release which is correlated to movement initiation, a sequence of events that is defective in the context of PD. Bursting activity is observed in vivo (Otomo et al., 2020) but also in *ex vivo* tissue by exogenous applications of NMDA in combination to a SK channel blocker (Seutin et al., 1993; Destreel et al., 2019; Soden et al., 2013), by glutamate applications or synaptic stimulation (Blythe et al., 2007; Hage and Khaliq, 2015).

In addition to glutamate, a co-agonist such as glycine (Johnson and Ascher, 1987) or D-serine (Kleckner and Dingledine, 1988) is an absolute requirement for NMDAR channel opening (Currás and Pallotta, 1996). While both amino acids have been shown to serve as endogenous agonists at the NMDAR glycine site, the contribution of the one or the

* Corresponding author.
E-mail address: dominique.engel@uliege.be (D. Engel).
[1] Lead contactFurther information and requests for resources should be directed to and will be fulfilled by the lead contact, Dominique Engel

https://doi.org/10.1016/j.pneurobio.2025.102773
Received 19 December 2024; Received in revised form 17 March 2025; Accepted 24 April 2025
Available online 26 April 2025

other is dependent on neuronal development (Le Bail et al., 2015), expression of specific GluN2 subunits (Le Bail et al., 2015; Papouin et al., 2012) and level of synaptic activity (Li et al., 2013). D-serine is generally associated to the synaptic site where GluN2A-containing NMDARs are preferentially expressed, and glycine to the extrasynaptic site where GluN2B-containing NMDARs are present (Papouin et al., 2012). In SNc DA neurons, both EPCSs and bursts can be potentiated by exogenous co-agonists or by the blockade of glycine uptake (Destreel et al., 2019) indicating that the co-agonist site of NMDARs is not saturated. In addition, blockade of the co-agonist binding-site on NMDARs abolished bursts, revealing the importance of the co-agonist in this firing pattern (Destreel et al., 2019). However, the identity of the endogenous co-agonist as well as the pool of NMDARs involved in burst generation remain unknown.

In this study, we determined the location of the NMDAR pool and the identity of the co-agonist implicated in the generation of bursting activity in SNc DA neurons. Our findings reveal that the pool of NMDARs located outside synapses is recruited to generate bursting together with the co-agonist glycine. The distribution of the co-agonists within and outside synapses is similar to other excitatory synapses as D-serine activates synaptic NMDARs. Extrasynaptic NMDARs are activated by spillover of glutamate during sustained synaptic transmission. These findings shed light on how the spatial distribution of NMDARs and their associated co-agonists influences burst generation in SNc DA neurons.

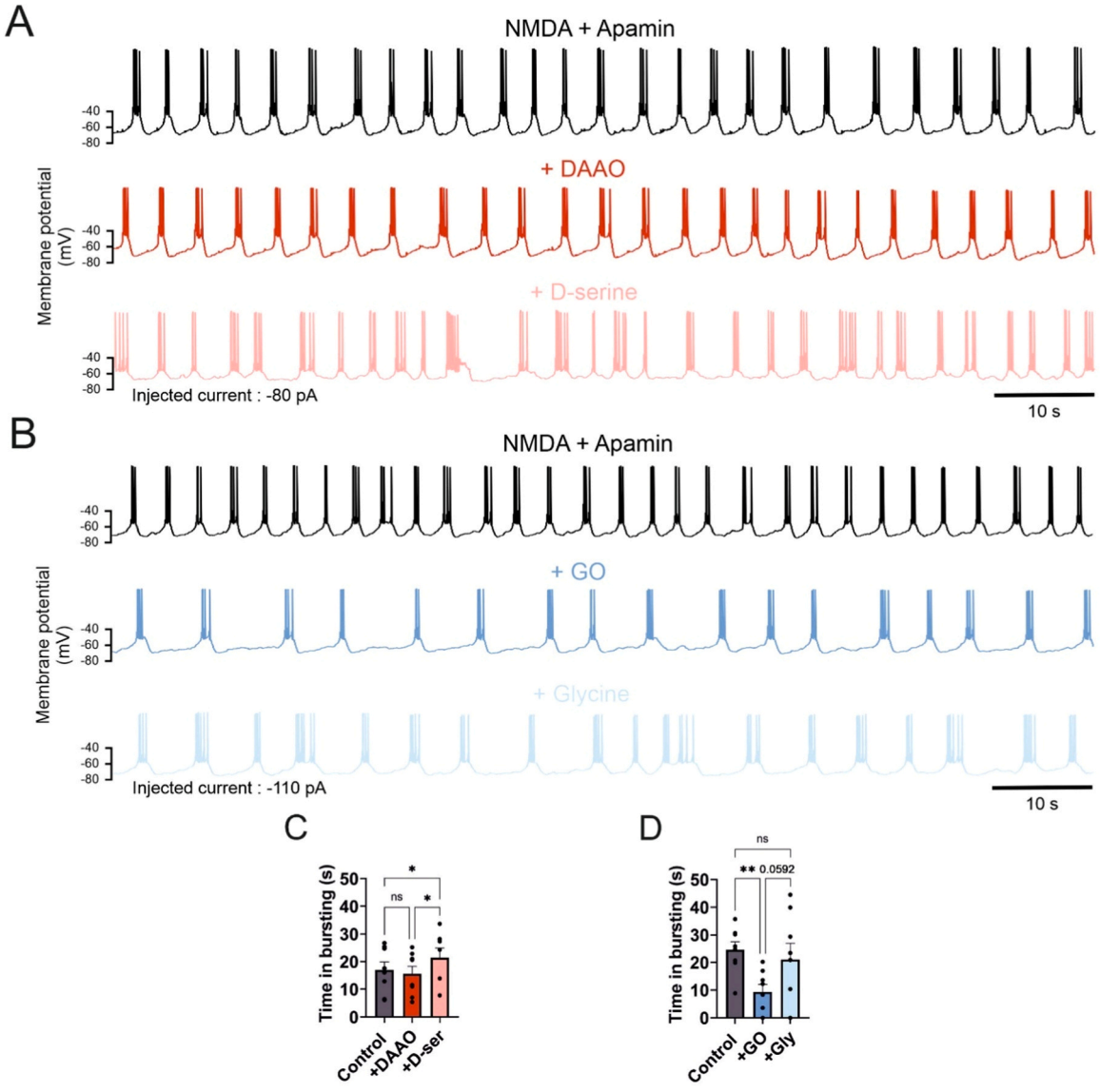

Fig. 1. Glycine controls the time spent in bursting. A, Voltage traces from a SNc DA neuron in the presence of NMDA and apamin (top trace black), following incubation with DAAO (45 min, 0.2 units/ml; middle trace red) and with DAAO supplemented by D-serine (100 μM, bottom trace light red). B, Voltage traces as in A top (trace black), following treatment with GO (45 min, 0.2 units/ml; middle trace blue) and with GO+glycine (1 mM, bottom trace light blue). C, Summary plot showing the time in bursting in control (grey), in DAAO (red) and in DAAO+D-serine (100 μM, light red). Control: 17.0 ± 2.9 s; DAAO: 15.6 ± 2.7 s; DAAO+D-serine: 21.4 ± 3.6 s. Time in bursting was unchanged in DAAO (ns versus control), but increased in DAAO+D-serine ($p < 0.05$ for DAAO+D-serine versus DAAO and for DAAO+D-serine versus control). Data points are in control, n = 8; DAAO, n = 8; DAAO+D-serine, n = 8. D, Summary plot showing the time in bursting in control (grey), in GO (blue) and in GO+glycine (light blue). Control: 24.6 ± 2.9 s; GO: 9.4 ± 2.7 s; GO+glycine: 21.1 ± 6.0 s. Time in bursting was significantly decreased in GO ($p < 0.01$ for control versus GO), increased in tendency in GO+glycine ($p = 0.0592$ for GO+glycine versus GO) but similar as in control (ns for GO+glycine versus control). Data points are in control, n = 8; GO, n = 8; GO+glycine, n = 8. Bars represent mean ± SEM; points indicate data from individual experiments. The p values are from Anova followed by post hoc Tukey's test (C-D), with ns [not significant], $^{*}p < 0.05$ and $^{**}p < 0.01$.

2. Results

2.1. Co-agonist glycine activates NMDARs to regulate bursting activity

Bursting activity in SNc DA neurons relies on the tonic activation of NMDARs (Chergui et al., 1993) through the binding of the neurotransmitter glutamate. In addition to this main agonist, a co-agonist such as glycine or D-serine participates to the activation of NMDARs as the blockade of the co-agonist site abolishes bursts (Destreel et al., 2019). However, which endogenous co-agonist is predominant to activate NMDARs during this phasic activity remains unknown. To identify the co-agonist activating NMDARs implicated in burst generation, enzymatic depletion of each of the potential co-agonists was combined to patch-clamp recordings in acute brain slices. DA neurons were identified in current- and voltage-clamp and using post hoc immunohistochemistry for tyrosine hydroxylase (Fig. S1). Bursting activity was induced by bath application of NMDA and apamin and hyperpolarizing current injection in DA neurons (Destreel et al., 2019). Slices were incubated for 45 minutes with either D-amino acid oxidase (DAAO) (Fig. 1 A) or glycine oxidase (GO) (Fig. 1B) to degrade D-serine or glycine, respectively. While the application of DAAO did not affect the bursting activity (Fig. 1 C and Table S1), the incubation with GO strongly reduced the time a neuron spend in burst firing (Fig. 1D and Table S1). Adding D-serine to DAAO-treated slices increased the time in burst firing (Fig. 1 C and Table S1) in comparison to treatment with DAAO alone but also in comparison to control conditions. Supplementing glycine to GO-treated samples increased with a strong tendency the time spent in bursting and almost restored the time in busting when comparing to control conditions (Fig. 1D and Table S1). The stronger effect of D-serine to increase the time in bursting in comparison to glycine might be due to a powerful uptake of glycine (Destreel et al., 2019). These results indicate that the co-agonist glycine controls the time DA neurons spend in bursting phase through the activation of NMDARs.

To control for changes in the amount of glycine and D-serine in slices in the presence of either GO or DAAO, concentrations of glycine and D-serine were evaluated using high-performance liquid chromatography

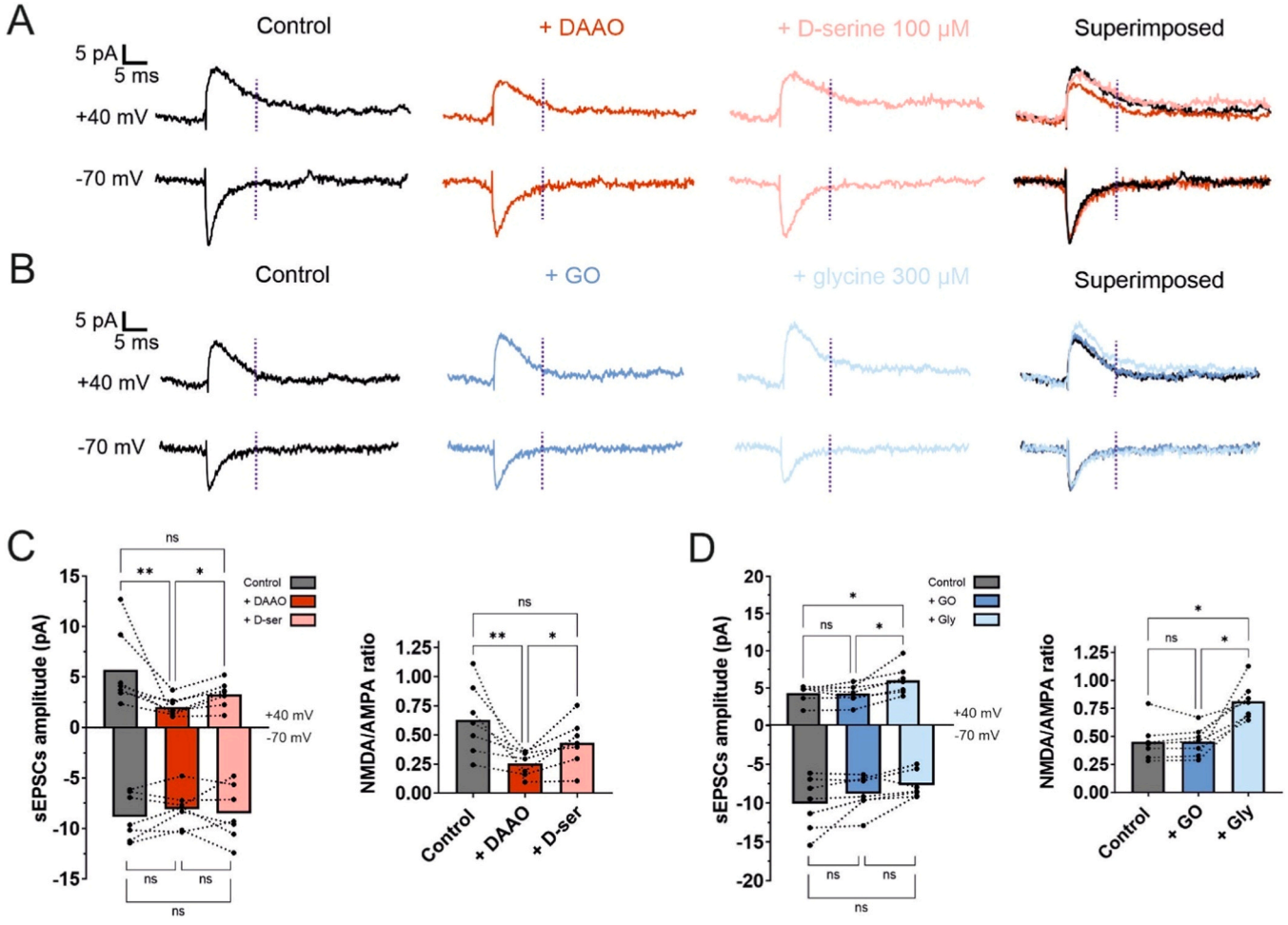

Fig. 2. D-serine is the main co-agonist of synaptic NMDARs in SNc DA neurons. A, Averaged traces (~100 events) of sEPSCs at + 40 mV (upper traces) and −70 mV (lower traces) in control, in DAAO (45 min, 0.2 units/ml) and in DAAO+D-serine (100 µM). At the right are superimposed traces for the three conditions. Amplitude of NMDAR-mediated component was measured at +40 mV (vertical dashed lines). B, Averaged traces (~100 events) of sEPSCs at +40 mV and −70 mV in control, in GO (45 min, 0.2 units/ml) and in GO+glycine (1 mM). Superimposed traces are at the right. C, Summary bar graph of traces recorded as in (*A*). At +40 mV, control: 5.7 ± 1.4 pA; DAAO: 2.0 ± 0.4 pA; DAAO+D-serine: 3.3 ± 0.5 pA. NMDAR-sEPSCs were decreased in DAAO ($p < 0.01$ versus control), increased in DAAO+D-serine ($p < 0.05$ versus DAAO) but similar as in control (ns for DAAO+D-serine versus control). At −70 mV, control: −8.8 ± 0.9 pA; DAAO: −8.1 ± 0.7 pA; DAAO+D-serine: −8.5 ± 1.0 pA. AMPAR-sEPSCs were unchanged under any conditions (ns). Data points are: Control, n = 7; DAAO, n = 7; DAAO+D-serine, n = 7. D, Summary bar graph of traces recorded as in B. At +40 mV, control: 4.3 ± 0.4 pA; GO: 4.3 ± 0.5 pA; GO+glycine: 6.0 ± 0.7 pA. NMDAR current was unchanged in GO (ns versus control), but increased in GO+glycine ($p < 0.05$ for GO+glycine versus GO and GO+glycine versus control). At −70 mV, control: −10.1 ± 1.3 pA; GO: −8.8 ± 0.9 pA; GO+glycine: −7.7 ± 0.6 pA. Currents were unchanged (ns). Data points are: Control, n = 7; GO, n = 7; GO+glycine, n = 7. C-D, Bars represent mean ± SEM; points indicate data from individual experiments. The p values are from Friedman test followed by Dunn's post hoc test (data at +40 mV in C-D) or from Anova 1 test followed by Tukey's post hoc test (data at −70 mV in C-D).

(HPLC) experiments. In slices incubated with either DAAO or GO, D-serine and glycine concentration were significantly decreased, confirming that DAAO and GO specifically degrade D-serine and glycine, respectively (Fig. S2). The specificity of the enzymes observed here is in line with previous observations in comparable experimental conditions (Le Bail et al., 2015; Papouin et al., 2012; Li et al., 2013) and indicate that the reduction of time in bursting is due to a selective reduction of the respective co-agonist amount.

2.2. Synaptic NMDARs are activated by the co-agonist D-serine

The nature of the endogenous co-agonist activating the synaptic pool of NMDARs has not been identified for SNc DA neurons. Incubation of slices with DAAO induced a significant reduction in peak amplitude of

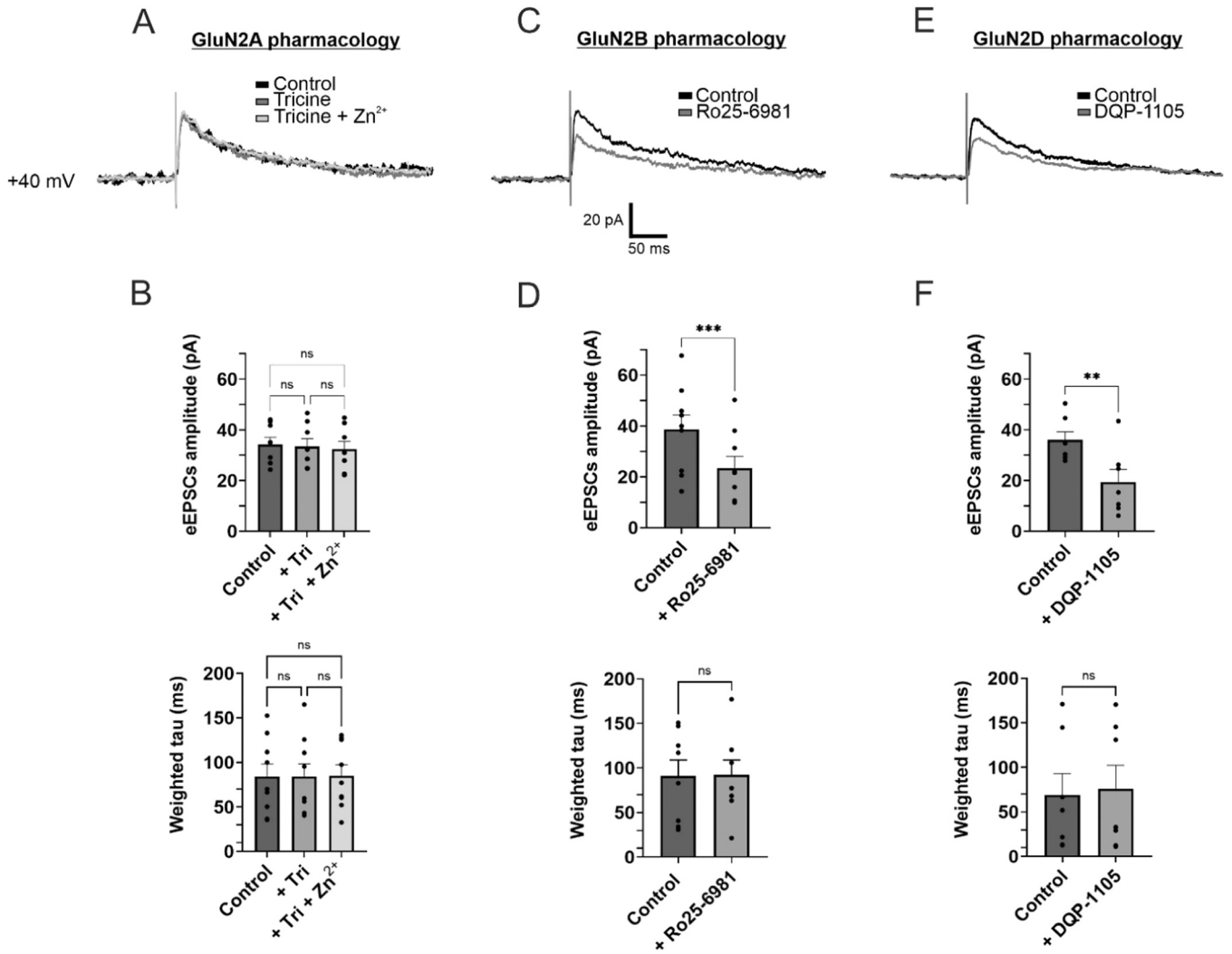

Fig. 3. Subunit composition of synaptic NMDARs in nigral DA neurons. A, Averaged eEPSCs (~30 events) recorded from SNc DA neurons at +40 mV in control conditions (black traces), after incubation with tricine (gray trace) and subsequently after tricine+Zn^{2+} (light grey trace). A focal double-barreled stimulating electrode was placed rostrally to the SN to activate fibers from the STN. For each condition traces were recorded in the presence of picrotoxin (50 μM), CGP 55485 (1 μM), CNQX (10 μM), and strychnine (10 μM). Tricine was used at 10 mM and Zn^{2+} at 60 μM (to have 300 nM free Zn^{2+}) (Vergnano et al., 2014). B, Bar chart for the mean amplitude of NMDAR-eEPSCs (top) in control conditions (dark grey bar), in tricine (grey bar) and in tricine+Zn^{2+} (light grey bar). At +40 mV, control: 34.2 ± 2.8 pA; tricine: 33.5 ± 3.0 pA; tricine+Zn^{2+}: 32.4 ± 3.0 pA. NMDAR-mediated current was neither modified in tricine (ns versus control) nor in tricine+Zn^{2+} (ns for tricine+Zn^{2+} versus tricine and for tricine+Zn^{2+} versus control). Bar chart for the weighted decay time constant of the NMDAR-eEPSCs (bottom) in control conditions (dark grey bar), in tricine (grey bar) and in tricine+Zn^{2+} (light grey bar). Weighted decay, control: 84.0 ± 14.1 ms; tricine: 84.0 ± 14.3 ms; tricine+Zn^{2+}: 85.0 ± 12.2 ms. Decay of NMDAR current was neither modified in tricine (ns versus control) nor in tricine+Zn^{2+} (ns for tricine+Zn^{2+} versus tricine and for tricine+Zn^{2+} versus control). Data points are in control, n = 8; tricine, n = 8; tricine+Zn^{2+}, n = 8. **C,** Averaged eEPSCs (~30 events) recorded at +40 mV in control conditions (black traces) and in Ro25–6981 (grey traces). Ro25–6981 was used at 1 μM. **D,** Bar chart showing the mean amplitude of NMDAR-eEPSCs (top) in control conditions (dark grey bar) and in Ro25–6981 (grey bar). At +40 mV, control: 38.6 ± 5.7 pA; Ro25–6981: 23.4 ± 4.7 pA. NMDAR current amplitude was decreased in Ro25–6981 ($p < 0.001$ versus control). Bar chart showing the weighted decay time constant of the NMDAR-eEPSCs (bottom) in control conditions (dark grey bar) and in Ro25–6981 (grey bar). Weighted decay, control: 91.0 ± 17.9 ms; Ro25–6981: 92.5 ± 16.4 ms). NMDAR current decay was not changed in Ro25–6981 (ns versus control). Data points are in control, n = 9; Ro25–6981, n = 9. **E,** Averaged eEPSCs (~30 events) recorded at +40 mV in control conditions (black traces) and in DQP-1105 (grey traces,top). DQP-1105 was used at 20 μM. **F,** Bar chart showing the amplitude of the NMDAR-eEPSCs (top) in control conditions (dark grey bar) and in DQP-1105 (grey bar). At +40 mV, control: 36.0 ± 3.2 pA; DQP-1105: 19.4 ± 5.0 pA). NMDAR current amplitude was decreased in DQP-1105 ($p < 0.01$ versus control). Bar chart showing the decay of the NMDAR-eEPSCs (bottom) in control conditions (dark grey bar) and in DQP-1105 (grey bar). Weighted decay, control: 68.8 ± 24.4 ms; DQP-1105: 76.1 ± 26.3 ms). NMDAR current decay was not changed in DQP-1105 (ns versus control). Data points are in control, n = 7; DQP-1105, n = 7. Bars represent mean ± SEM; points indicate data from individual experiments. The p values are from Anova test followed by Tukey's post hoc test (A-C) or from paired *t*-test (D-F).

the NMDAR-mediated component of spontaneous synaptic excitatory postsynaptic currents (sEPSCs) at +40 mV (Fig. 2 A). Addition of exogenous D-serine reversed the effects of DAAO on the amplitude of sEPSCs which was similar to the sEPSC amplitude in control (Fig. 2 C). Treatment with GO did not change the amplitude of sEPSCs but supplementation of glycine to GO-treated samples increased the amplitude of sEPSCs (Fig. 2B) which was significantly larger than in control conditions (Fig. 2D). The large increase in sEPSC amplitude is due to the high glycine concentration used to allow the co-agonist to reach the synaptic cleft bordered with glycine transporters (Berger et al., 1998). Currents at −70 mV, representing principally the activation of AMPARs, were not modified, either with DAAO or with GO (Fig. 2C-D). These results provide evidence that D-serine maintains synaptic activation of NMDARs in DA neurons. Unexpectedly, the co-agonist activating synaptic NMDARs and the pool of NMDARs for bursting differed in their identity. This indicates that the pool of NMDARs implicated in the generation of bursts might be different from the pool of synaptic NMDARs.

To reveal the identity of the co-agonist for an identified glutamatergic input, electrical stimulation was applied to fibers from the STN and evoked EPSCs (eEPSCs) recorded in DA neurons (Fig. S3). Incubation with DAAO reduced significantly the peak amplitude of the NMDAR-eEPSCs at +40 mV and addition of exogenous D-serine reversed the effects of DAAO on the amplitude of eEPSCs (Fig. S4A, C). Treatment with GO did not change the mean amplitude of eEPSCs but addition of glycine to GO-treated samples increased the mean amplitude of eEPSCs, which was significantly larger than in control conditions (Fig. S4B, D). Currents at −70 mV were neither changed by the treatment with DAAO, nor with GO. These results obtained for the STN-SNc synapse are similar to those observed on sEPSCs, indicating that the same co-agonist, D-serine, is probably shared by distinct excitatory inputs in DA neurons. In addition, these results further reveal that synaptic NMDARs and NMDAR-mediating bursts are activated by distinct co-agonists.

2.3. Excitatory synapses in nigral DA neurons are composed of triheteromeric NMDARs

An association between the nature of the predominant co-agonist and the expression of a specific synaptic GluN2 subunit has been reported (Le Bail et al., 2015; Papouin et al., 2012). To examine the subunit composition of NMDARs in DA neurons, GluN2 subunit specific NMDAR blockers were used. NMDARs containing the GluN2A subunit have been shown to be inhibited by Zn^{2+} via a high-affinity site for the divalent cation located on this subunit (Vergnano et al., 2014; Morabito et al., 2022). Tricine which is a selective chelator for zinc (Paoletti et al., 1997, 2009) should therefore relieve the inhibition of GluN2A-NMDARs and induce an augmentation of GluN2A-NMDAR-EPSCs (Vergnano et al., 2014). In DA neurons, application of the Zn^{2+} chelator tricine did not modify the amplitude of the NMDAR-eEPSCs at +40 mV (Fig. 3 A, B). Subsequent addition of Zn^{2+} was unable to change the amplitude of eEPSCs too. In prefrontal cortical layer 5 pyramidal neurons, however, in which GluN2A-containing NMDARs are present (Fossat et al., 2012; Balsara et al., 2014; Wang et al., 2008), application of tricine and tricine+Zn^{2+} increased and decreased, respectively the NMDAR-eEPSC amplitude (Fig. S5) illustrating previous observations for neurons expressing GluN2A (Vergnano et al., 2014; Morabito et al., 2022; Nozaki et al., 2011). In contrast, application of the antagonist of NMDARs containing GluN2B (Ro25–6981) reduced significantly the amplitude of eEPSCs to ~60 % of control (Fig. 3 C, D). Similarly application of the GluN2D-containing NMDAR antagonist DQP-1105 reduced the amplitude of eEPSCs to ~53 % of control (Fig. 3E, F). Weighted decay time constant of eEPSCs was neither modified by the application of Ro25–6981 nor by DQP-1105. This absence of effect on the decay time constant by either Ro25–6981 or DQP-1105 indicates that a high proportion of synaptic NMDARs in DA neurons are triheteromeric GluN1/GluN2B/GluN2D receptors, making unlikely the participation of diheteromeric GluN1/GluN2B and GluN1/GluN2D receptors (Yi et al., 2019; Brothwell et al., 2008). Previous studies have demonstrated that recombinant diheteromeric GluN1/GluN2B and GluN1/GluN2D NMDARs produce respectively a substantially faster and slower deactivation time constant in comparison to the deactivation time constant of a recombinant GluN1/GluN2B/GluN2D receptor which is intermediate (Yi et al., 2019). if diheteromeric GluN1/GluN2B and/or GluN1/-GluN2D receptors would be present in the membrane, the application of Ro25–6981 or DQP-1105 would be expected to change the decay time course of NMDAR-EPSCs. The absence of change in the decay time constant of EPSCs suggests that triheteromeric GluN1/GluN2B/GluN2D receptors represent a large population of NMDARs (Yi et al., 2019; Brothwell et al., 2008; Harris and Pettit, 2007; Gibb, 2022). Taken together, these results suggest the presence of triheteromeric NMDARs containing GluN2B and GluN2D but not GluN2A in synapses of SNc DA neurons.

The expression of NMDAR subunits in DA neurons was further explored using immunohistochemistry for GluN2A, GluN2B and GluN2D subunits. The distribution of the subunits was determined in TH^+ DA neurons in the region in which DA neurons were selected for patch-clamp recordings (Fig. S6). Both GluN2B and GluN2D subunits were present in a large majority (~80 %) of TH^+ neurons but the GluN2A subunit was only present in ~20 % of TH^+ neurons (Fig. S6B, C). Within TH^+ neurons, there were ~3 times more fluorescent dots for GluN2B and GluN2D subunits than for GluN2A subunits (Fig. S6D). The distribution of the three distinct NMDARs subunits was further examined at higher magnification at the cellular level by taking into account membrane and intracellular locations (Fig. S7). Immunolabeling for GluN2B and GluN2D subunits was found predominantly at the membrane (GluN2B membrane, ~75 % of the total dots; GluN2D membrane, ~77 % of the total dots) in comparison to the intracellular compartment (GluN2B intracellular, ~25 % of the total dots; GluN2D intracellular, ~23 %). In contrast, the distribution of GluN2A was inverted and found at a high proportion in cell's intracellular milieu (GluN2A intracellular, ~85 %) and at a very low proportion at the membrane (GluN2A membrane, ~15 %) (Fig. S7A, B). This GluN2 subunits expression profile is consistent with the pharmacological data obtained using subunit specific NMDAR blockers (Fig. 3).

2.4. Glycine controls the activation of the NMDAR-mediated tonic current

NMDARs are generally concentrated in synapses but are also encountered at extrasynaptic sites (Petralia et al., 2010). Activation of extrasynaptic NMDARs by ambient glutamate generates a whole-cell tonic current manifested by the blockade of NMDARs (Le Meur et al., 2007). This NMDAR-mediated tonic current has been described in SNc DA neurons (Wild et al., 2015) but the preferred co-agonist for this NMDAR-mediated current remains undetermined. In slices incubated with DAAO, the amplitude of the tonic current recorded at V_{hold} = +40 mV was not significantly different from control after application of D-AP5 (Fig. 4 A, B). In contrast, in the presence of GO, the amplitude of the tonic current was reduced to ~46 % of control, indicating that reducing the amount of glycine impaired the activation of NMDARs mediating this current. Remarkably, since glycine is the predominant co-agonist for extrasynaptic NMDARs activated during tonic current and is also controlling the occurrence of bursts, this pool of NMDARs might be critical for the generation of bursts.

To determine the subunit composition of extrasynaptic NMDARs in DA neurons, subunit specific NMDAR blockers were used. In the presence of tricine, the magnitude of the tonic current was similar as in control conditions (Fig. 4B, C). Adding Zn^{2+} to tricine did not modify the current amplitude too, indicating that the GluN2A subunit may not be a component of extrasynaptic NMDARs. The GluN2B blocker Ro25–6981 and the GluN2D blocker DQP-1105 reduced significantly the tonic current to ~31 % of control and ~26 % of control, respectively (Fig. 4B, C).

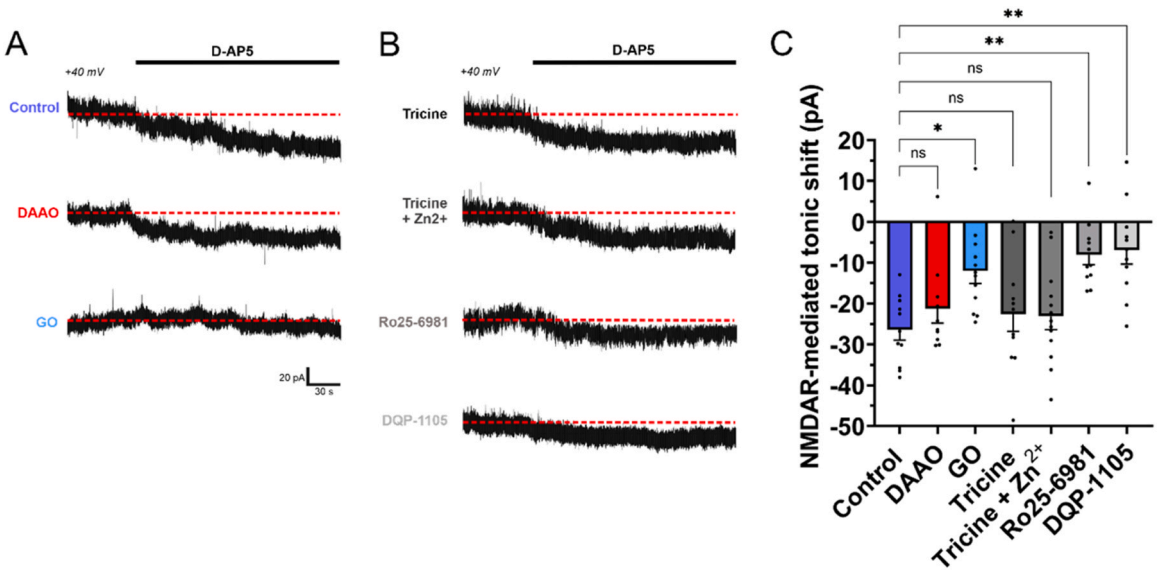

Fig. 4. Glycine gates extrasynaptic NMDARs in nigral DA neurons. A, Tonic NMDAR-mediated current in control conditions (top), in DAAO (45 min, 0.2 units/ml; below middle) and in GO (45 min, 0.2 units/ml; bottom) revealed by the current shift induced by D-AP5 at V_{hold} = +40 mV. Dashed red line indicate amplitude of holding current before the application of D-AP5. Data in the different conditions are from distinct experiments. B, Tonic NMDAR-mediated current in tricine (10 mM, top), in tricine+Zn^{2+} (60 μM, second from top), in Ro25–6981 (1 μM, third from top) and in DQP-1105 (20 μM, bottom). **C,** Summary bar graph of the mean amplitude of the NMDAR-mediated tonic current. Control: −26.5 ± 2.5 pA; DAAO: −21.3 ± 3.5 pA; GO: −12.1 ± 3.0 pA; tricine: −22.6 ± 4.2 pA; tricine + Zn^{2+}: −23.1 ± 3.2 pA; Ro25–6981: −8.1 ± 2.4 pA; DQP-1105: −6.9 ± 3.5 pA. NMDAR-mediated tonic current was unchanged in DAAO, in tricine and in tricine+ Zn^{2+} (ns versus control), but reduced in GO ($p < 0.05$ versus control), in Ro25–6981 and in DQP-1105 ($p < 0.01$ versus control). Data points are in control, n = 11; DAAO, n = 10; GO, n = 12; tricine, n = 11; tricine+Zn^{2+}, n = 13; Ro25–6981, n = 11; DQP-1105, n = 11. Bars represent mean ± SEM; points indicate data from individual experiments. The p values are from Kruskal-Wallis test followed by a post hoc Dunn's test.

These results indicate that extrasynaptic NMDARs may be composed by GluN2B and GluN2D subunits, as observed for juvenile tissue (Jones and Gibb, 2005) and that extrasynaptic, like synaptic sites, may express a high proportion of triheteromeric GluN1/GluN2B/GluN2D receptors (Brothwell et al., 2008). Taken together, our results strongly suggest that even though the same NMDAR subtype is present at synaptic and extrasynaptic sites, distinct co-agonists are responsible for their activation.

2.5. *Activation of extrasynaptic NMDARs generates tonic current*

It is generally accepted that the tonic NMDAR-mediated current is largely due to the activation of extrasynaptic NMDARs (Le Meur et al., 2007). To evaluate the potential contribution of synaptic NMDARs to the current, the irreversible open channel blocker MK-801 was used to block specifically synaptic NMDARs (Huettner and Bean, 1988; Koh et al., 2022; Liu et al., 2013). After a 20 min application of MK-801, low frequency stimulation elicited eEPSCs at +40 mV with strongly reduced amplitude to ~30 % of control (Fig. 5 A). The consecutive application of D-AP5 revealed a tonic current with an amplitude similar to the amplitude measured without the inhibition of synaptic NMDARs (Fig. 5 A, C). In contrast, the blockade of both synaptic and extrasynaptic NMDARs under MK801 incubation at +40 mV strongly reduced the amplitude of the tonic current (Fig. 5B, C). The absence of a change in the tonic current when synaptic NMDARs are blocked indicates that the pool of extrasynaptic NMDARs mainly sustains the tonic NMDAR-mediated current in DA neurons.

2.6. *Bursting activity relies on the contribution of extrasynaptic NMDARs*

In vivo, bursting activity in SNc DA neurons has been reported to result from the tonic activation of NMDARs (Chergui et al., 1993), but which pool of NMDARs contribute to this firing activity is not known. To determine the potential contribution of synaptic NMDARs to bursting activity, MK-801 was applied. In the presence of the inhibitor, the amplitude of eEPSCs at +40 mV was strongly reduced, indicating that a large fraction of synaptic NMDARs were blocked (Fig. 6 A). The recording configuration was then switched to current-clamp to determine whether the spontaneous bursting activity can be induced. After a short time period (~10 min) to allow stabilization of the membrane potential, NMDA and apamin were bath-applied in combination with a DC current injection. In these conditions, DA neurons exhibited spontaneous bursting activity, comparable to the activity recorded without the blockade of synaptic NMDARs (Fig. 6B-E). These results strongly suggest that bursts in DA neurons are elicited mainly by the activation of extrasynaptic NMDARs.

2.7. *Synaptic glutamate released from STN fibers allows burst generation via extrasynaptic NMDARs*

In vivo, the stimulation of the glutamatergic STN neurons favors bursting (Chergui et al., 1994). To evaluate with pool of NMDARs is implicated for burst at the STN-SNc synapse, tract stimulation was applied to fibers originating from STN and voltage recorded in DA neurons. A train of stimuli at low frequency (10 Hz) did not evoke associated APs (Fig. 7 A, C-E), presumably because at this stimulation frequency, extrasynaptic NMDARs are not recruited by spillover (Harris and Pettit, 2008). Incubation with either DAAO or GO or GO+glycine was also unable to modify the firing. In contrast, stimulation at a higher frequency (50 Hz) for 500 ms induced in control conditions and in the presence of DAAO short bursts (Fig. 7B) which were similar in both conditions. In the presence of GO, bursts had a reduced number of AP, a decreased intraburst frequency but an increased time to first AP. In contrast, supplementation of glycine to GO induced burst at 50 Hz, increased the AP number, intraburst frequency and decreased time to first AP in comparison to the condition in which GO was alone (Fig. 7B, C-E). At this stimulation frequency (50 Hz), extrasynaptic NMDARs may be recruited by spillover of glutamate (Harris and Pettit, 2008) and co-activated by glycine. To further evaluate the contribution of glutamate spillover to bursting glutamate uptake blockade was applied in

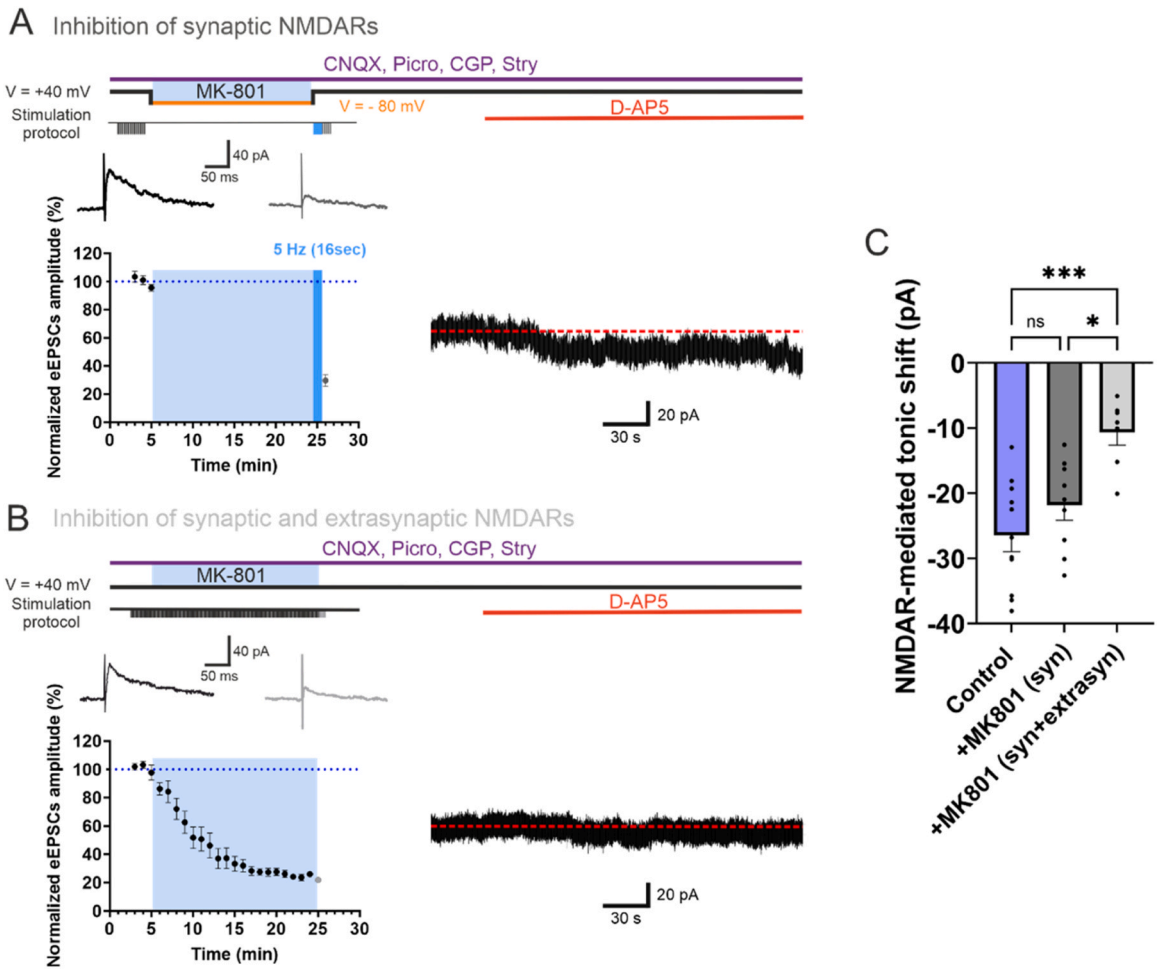

Fig. 5. Extrasynaptic NMDARs mediate tonic current in SNc DA neurons. A, Experimental protocol to block synaptic NMDARs using MK-801. Averaged eEPSC at V_{hold} = +40 mV under low stimulation frequency (0.1 Hz). Switch to current-clamp (CC, V_{hold} ~ −80 mV) for ~20 min during the application of MK-801 (20 μM). Washout of MK-801 and switch back to V_{hold} = +40 mV. Stimulation was resumed using a frequency of 5 Hz for 16 s (Koh et al., 2022; Yang et al., 2017). Note the very strong reduction of the NMDAR-eEPSC amplitude after MK-801. Neuron was kept at V_{hold} = +40 mV and D-AP5 (50 μM) was applied. During the whole experiment, CNQX (10 μM), picrotoxin (50 μM), CGP 55485 (1 μM) and strychnine (10 μM) were present in the bath. B, Experimental design to block both synaptic NMDARs and extrasynaptic NMDARs using MK-801. During application of MK-801, holding potential was kept at +40 mV and repetitive afferent fiber stimulation frequency was at 0.2 Hz. Note the *quasi* absence of the tonic current after application of D-AP5. C, Summary bar graph of the peak amplitude of the tonic current. Control: −26.5 ± 2.5 pA; after MK-801 treatment to reduce synaptic NMDARs (syn): −21.8 ± 2.3 pA; after MK-801 treatment and continuous synaptic stimulation to block synaptic and extrasynaptic NMDARs (syn+extrasyn): −10.6 ± 2.0 pA). Tonic current was not different after MK-801 [syn] (ns versus control) but was decreased after MK-801 [syn+extrasyn] ($p < 0.05$ for MK-801 [syn] versus MK-801 [syn+extrasyn] and $p < 0.001$ for MK-801 [syn+extrasyn] versus control). Data points are in control, n = 11; +MK-801 (syn), n = 9; +MK-801 (syn+extrasyn), n = 7. Bars represent mean ± SEM; points indicate data from individual experiments. The p values are from Anova test followed by a post hoc Tukey's test, with $^{***}p < 0.001$.

order to allow glutamate to escape from the synaptic cleft and to reach extrasynaptic sites (Arnth-Jensen et al., 2002; Asztely et al., 1997; Harney et al., 2008). At 10 Hz, tract stimulation induced high firing in the presence of the glutamate uptake blocker TBOA and in TBOA supplemented by glycine (Fig. S8A, C-E). At 50 Hz, synaptic stimulation induced even stronger bursting in TBOA and in TBOA+glycine (Fig. S8B, C-E), confirming the role of glutamate spillover in the induction of bursting. Overall, these results highlight that at extrasynaptic locations, spilling over of glutamate from the synapse and glycine activate NMDARs to switch on a burst in SNc DA neurons.

3. Discussion

The contribution of NMDARs located at synaptic or extrasynaptic sites and the availability of co-agonists within and outside synapses strongly influence the excitability of DA neurons and therefore the downstream release of dopamine in the dorsal striatum. Here, by using electrophysiological and biochemical experiments, we determined the nature of the co-agonist and the pool of NMDARs implicated in bursts generated by SNc DA neurons. First, we identified glycine as the co-agonist controlling the bursting time. Second, we observed that D-serine acts for glutamatergic synaptic transmission and not for bursting. Third, we found that glycine is implicated in the activation of extrasynaptic NMDARs and in bursting. Fourth, we showed that the tonic NMDAR-mediated current is predominantly mediated by extrasynaptic NMDARs. Fifth, bursting activity is supported principally by the contribution of extrasynaptic but not synaptic NMDARs during glutamate spillover. Sixth, pharmacological experiments revealed that a substantial population of NMDARs are triheteromeric GluN1/GluN2B/GluN2D receptors, expressed both at synaptic and extrasynaptic sites. We concluded that the activation of glycine-gated extrasynaptic NMDARs by spillover of glutamate switch on bursting in DA neurons.

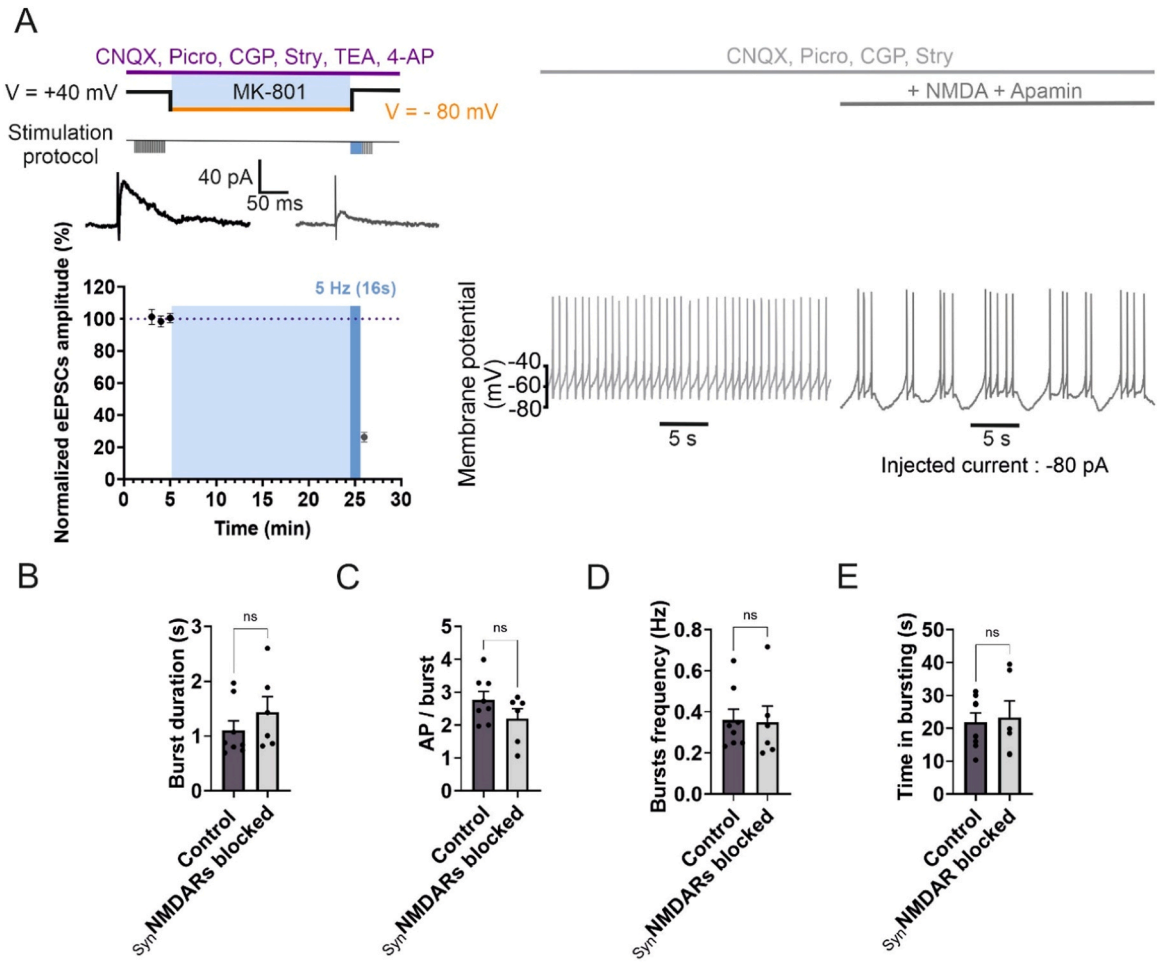

Fig. 6. Extrasynaptic NMDARs mediate bursting in SNc DA neurons. A, Blockade of synaptic NMDARs using MK-801. Control averaged eEPSC at V_{hold} = +40 mV. Switch to CC (V_{hold} = −80 mV) for ~20 min during the application of MK-801. Washout of MK-801 and switch back to V_{hold} = +40 mV. Stimulation was resumed. Bursting activity (right) recorded in CC induced by application of NMDA and apamin. To generate bursting in CC, CNQX (10 μM), picrotoxin (50 μM), CGP 55485 (1 μM) and strychnine (10 μM) were present in the bath. Note the presence of spontaneous bursts after the blockade of synaptic NMDARs. B, Summary plot showing burst duration in control and after the blockade of synaptic NMDARs. Control: 1.1 ± 0.2 s; $_{syn}$NMDARs blocked: 1.4 ± 0.3 ms. Burst duration was unchanged when synaptic NMDARs were blocked (ns versus control). C, Summary plot showing the number of AP/ burst in control and after the blockade of synaptic NMDARs. Control: 2.8 ± 0.3; $_{syn}$NMDARs blocked: 2.2 ± 0.3. AP number was not changed after synaptic NMDAR blockade (ns versus control). D, Summary plot showing burst frequency in control and after the blockade of synaptic NMDARs. Control: 0.4 ± 0.1 Hz; $_{syn}$NMDARs blocked: 0.4 ± 0.1 Hz. Burst frequency was not different after synaptic NMDAR blockade (ns versus control). E, Summary plot showing the time in bursting in control and after the blockade of synaptic NMDARs. Control: 21.9 ± 2.8 Hz; $_{syn}$NMDARs blocked: 23.3 ± 5.0 Hz. Burst frequency was not different after synaptic NMDAR blockade (ns versus control) (*C-E*) Data points are in control, n = 8; $_{syn}$NMDARs blocked, n = 6. Bars are mean ± SEM; points indicate data from individual experiments. The statistical tests used were Mann-Whitney test (B) or unpaired *t*-test (C- E).

3.1. NMDAR subtypes at synaptic and extrasynaptic locations in SNc DA neurons

NMDARs located at extrasynaptic versus synaptic sites have been shown to have different subunit compositions and to deserve distinct cellular functions (Hardingham and Bading, 2010). In adolescent SNc DA neurons, synaptic NMDARs are composed of GluN2B and GluN2D subunits, an expression pattern already observed at postnatal ages (Brothwell et al., 2008). Neither GluN2A (Brothwell et al., 2008; Jones and Gibb, 2005) nor GluN2C (Jones and Gibb, 2005) have been reported to be expressed in SNc DA neurons, either in the synaptic (Brothwell et al., 2008) or in extrasynaptic membrane (Jones and Gibb, 2005). NMDAR-eEPSCs were reduced in amplitude to ~60 % of control and ~50 % of control by the GluN2B-containing NMDAR blocker Ro25–6981 and the GluN2D-containing NMDAR blocker DQP-1105, respectively. These percentages of inhibition are comparable to those reported by previous observations for midbrain neurons (Harnett et al., 2009; Swanger et al., 2015) and hippocampal interneurons (Yi et al., 2019) in which GluN1/GluN2B/GluN2D triheteromers are present. A small proportion of diheteromeric GluN1/GluN2B or GluN1/GluN2D NMDARs might participate to the synaptic current, but the absence of change of the decay time course of NMDAR-eEPSCs in the presence of either Ro25–6981 or DQP-1105 argues against the presence of these diheteromeric NMDARs (Brothwell et al., 2008; Harris and Pettit, 2007; Perszyk et al., 2016). Tricine and Zn^{2+} were ineffective to modify NMDAR-eEPSC amplitude, indicating the absence of GluN2A in synaptic receptors. At extrasynaptic locations, the same NMDAR subtype is expressed as the one at synaptic locations, indicating a substantial proportion of triheteromeric GluN1/GluN2B/GluN2D NMDARs at both synaptic and extrasynaptic sites. The presence of GluN2B and GluN2D subunits is generally observed at extrasynaptic sites in distinct types of neurons in postnatal (Jones and Gibb, 2005; Harney et al., 2008; Lozovaya et al., 2004; Brickley et al., 2003) and in mature tissue (Riebe et al., 2016; Momiyama, 2000). The presence of GluN2B in synaptic NMDARs has also been observed in the hippocampus (Harris and Pettit, 2007) associated to GluN2A (Harris and Pettit, 2007; Rauner and Köhr,

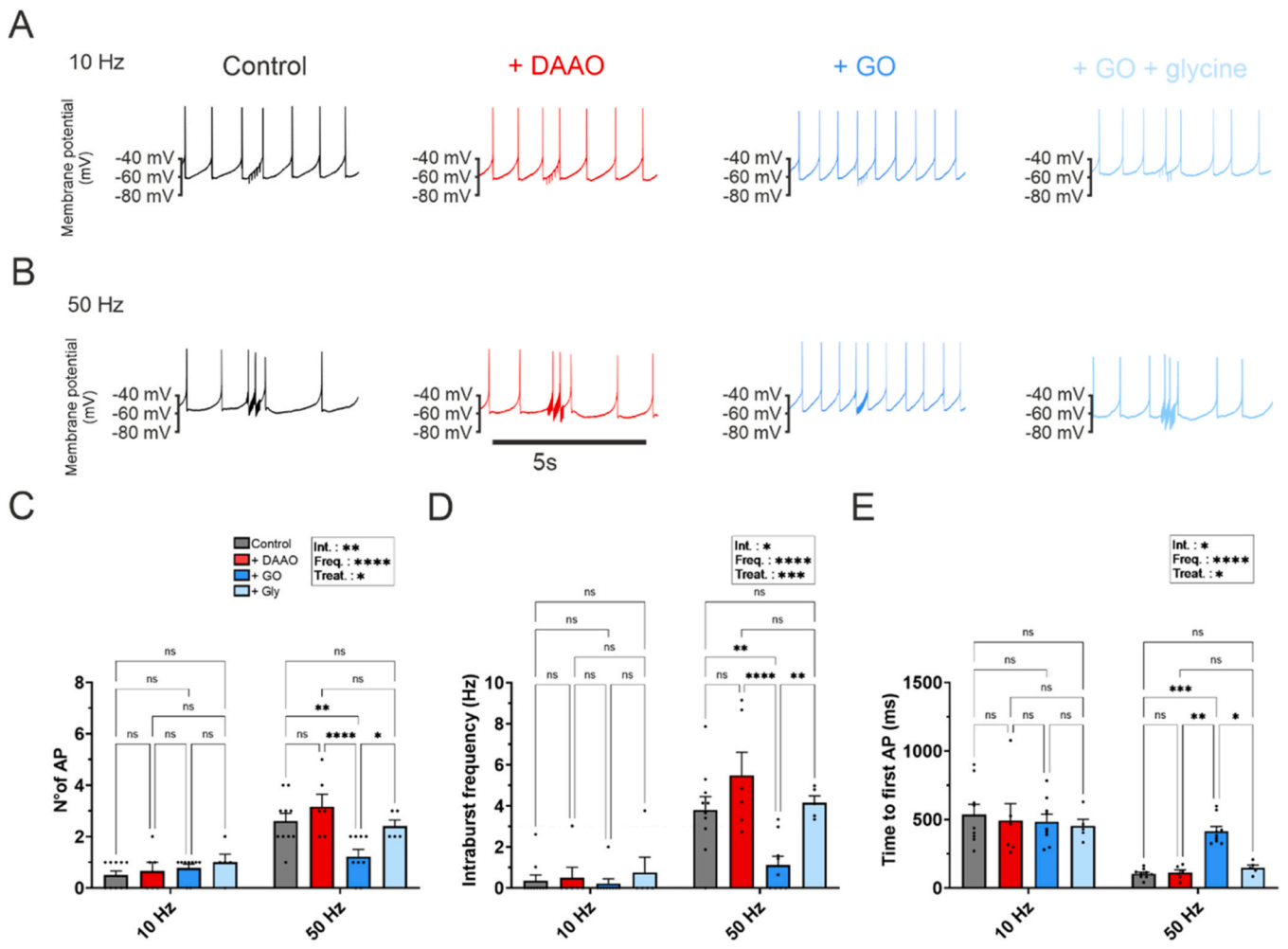

Fig. 7. Bursting activity requires glycine and glutamate spillover during high regime of synaptic transmission. A, Voltage traces in CC from a SNc DA during synaptic stimulation at 10 Hz for 500 ms in control (left), in DAAO (45 min, 0.2 units/ml, middle left), in GO (45 min, 0.2 units/ml, middle right) and in GO+glycine (1 mM, right). Voltage traces were recorded with CNQX (10 μM), picrotoxin (50 μM), CGP 55485 (1 μM) and strychnine (10 μM). B, Voltage traces in a SNc DA during synaptic stimulation at 50 Hz for 500 ms in control (left), in DAAO (middle left), in GO (middle right) and in GO+glycine (right). C, Summary plot showing the mean number of APs generated during stimulation at 10 Hz (left). Control: 0.5 ± 0.2; DAAO: 0.7 ± 0.3; GO: 0.8 ± 0.2; GO+glycine: 1.0 ± 0.3. AP number was unchanged under any conditions (ns). AP number for synaptic stimulation at 50 Hz (right). Control: 2.6 ± 0.3; DAAO: 3.2 ± 0.5; GO: 1.2 ± 0.3; GO + glycine: 2.4 ± 0.3. AP number was not different in DAAO and in GO+glycine (ns versus control) but was decrease in GO ($p < 0.01$ for GO versus control and $p < 0.0001$ for GO versus DAAO). AP number was increased in GO+glycine in comparison to GO ($p < 0.05$). D, Summary plot for the intraburst frequency during stimulation at 10 Hz (left). Control: 0.4 ± 0.3 Hz; DAAO: 0.5 ± 0.5 Hz; GO: 0.2 ± 0.2 Hz; GO + glycine: 0.8 ± 0.7 Hz. Intraburst frequency was unchanged under any conditions (ns). Intraburst frequency for stimulation at 50 Hz (right). Control: 3.8 ± 0.7 Hz; DAAO, 5.5 ± 1.3 Hz; GO, 1.1 ± 0.4 Hz; GO + glycine, 4.2 ± 0.3 Hz. Intraburst frequency was not different in DAAO and in GO+glycine (ns versus control) but was decreased in GO ($p < 0.01$ for GO versus control and $p < 0.0001$ for GO versus DAAO). Intraburst frequency was increased in GO+glycine in comparison to GO ($p < 0.01$). E, Summary plot showing the time to the first AP during stimulation at 10 Hz (left). Control: 536.4 ± 104.6 ms; DAAO: 491.6 ± 112.9 ms; GO: 483.4 ± 55.7 ms; GO+glycine: 452.0 ± 49.1 ms. Time to first AP was unchanged under any conditions (ns). Time to first AP for stimulation at 50 Hz (right). Control: 104.6 ± 11.8 ms; DAAO: 113.0 ± 19.9 ms; GO: 415.5 ± 33.8 ms; GO+glycine: 146.7 ± 20.6 ms. Time to first AP was not different in DAAO and in GO+glycine (ns versus control) but was increased in GO ($p < 0.001$ for GO versus control and $p < 0.0001$ for GO versus DAAO). Time to first AP was decreased in GO+glycine in comparison to GO ($p < 0.05$). C-E, Data points are in control, $n = 10$; DAAO, $n = 6$; GO, $n = 9$; GO+glycine, $n = 5$. Bars are means ± SEM; points indicate data from individual experiments. The p values are from Anova 2 followed by Tukey's post hoc Test.

2011) in pyramidal neurons to form triheteromeric receptors which represent a major population of NMDARs (Rauner and Köhr, 2011; Stroebel et al., 2018) and to GluN2D in interneurons (Yi et al., 2019; Perszyk et al., 2016). At extrasynaptic locations in the hippocampus GluN2B is associated to GluN2D (Harney et al., 2008; Lozovaya et al., 2004).

3.2. Location determines the identity of co-agonists

The identity of the co-agonist has been determined for several glutamatergic synapses in distinct principal neurons (Le Bail et al., 2015; Papouin et al., 2012; Li et al., 2013; Fossat et al., 2012; Panatier et al., 2006; Curcio et al., 2013). D-serine is generally engaged in the activation of synaptic NMDARs and our results confirms this rule for SNc DA neurons. In a unique case, however, glycine has been shown to activate synaptic NMDARs in mature dentate granule cells (Le Bail et al., 2015). The predominant role of D-serine for synaptic NMDARs has been associated to GluN2A-containing NMDARs for instance in adolescent cortical layer 5 neurons (Fossat et al., 2012) and hippocampal CA1 pyramidal neurons (Le Bail et al., 2015; Papouin et al., 2012). In the case of DA neurons, our results show that the preponderance of D-serine to activate synaptic NMDARs is however not accompanied by GluN2A- but by GluN2B-containing NMDARs. Enzymatic reduction of glycine revealed that this co-agonist predominates for the activation of extrasynaptic NMDARs in SNc DA neurons. A comparable correspondence has been reported for CA1 pyramidal neurons where glycine activates also

preferentially extrasynaptic GluN2B-containing NMDARs (Papouin et al., 2012). Is there consequently any possible influence exerted by a co-agonist on the NMDAR subunit composition? Interestingly, the GluN2B subunit in SNc DA neurons is present in the synaptic compartment, where D-serine is acting and in the extrasynaptic compartment where glycine operates, it seems that a direct influence of a preferred co-agonist on GluN2B or vice versa is unlikely. Furthermore, while both sites have NMDARs composed of GluN2B and GluN2D and D-serine and glycine have similar affinities for a given GluN2 subunit (Ferreira et al., 2017; Hansen et al., 2021), a discrimination between the two co-agonists cannot be operated by a GluN2B-containing NMDAR. Rather, the organization of the microenvironment, the presence of transporters for the co-agonists and the proximity of astrocytic leaflets in the vicinity of NMDARs certainly influences the predominant role of co-agonists at synaptic and extrasynaptic locations. The glycine transporter GLYT1 expressed in the SNc (Cubelos et al., 2005) might maintain a high concentration ratio of D-serine/glycine within the synaptic cleft and a low concentration ratio at the extrasynaptic membrane (Dopico et al., 2006). D-Serine reuptake by ASCT and EAAT transporters is not so efficient since they are not stereoselective and display low to moderate affinity for D-Serine. More work is needed to shed light on the establishment and role of the compartmentalization of co-agonists. Interestingly, co-agonists might represent an access to target synaptic versus extrasynaptic NMDAR pools.

3.3. Contribution of extrasynaptic NMDARs and glycine to bursting activity in SNc DA neurons

The pivotal role of NMDARs in the generation of bursts has been revealed using genetic inactivation of the GluN1 subunit in DA neuron (Wang et al., 2011; Zweifel et al., 2009). Both of these studies showed that inactivated NMDARs induced a decrease in bursting as observed in our work using depletion of glycine. Moreover, glycine is also preponderant for the activation of extrasynaptic NMDARs underlying for a large part the tonic NMDAR-mediated current. These results are in line with work showing that in vivo bursting is generated by tonically activated NMDARs (Chergui et al., 1993). Spontaneous bursting activity could be induced after the pharmacological blockade of synaptic NMDARs, further supporting the predominant contribution of extrasynaptic NMDARs to bursting. Altogether, these observations strongly suggest that the pool of NMDARs implicated in the generation of bursts and the pool of extrasynaptic NMDARs, both depending on glycine, correspond to the same pool of NMDARs. Functionally, how can extrasynaptic NMDARs be activated to generate bursts? This pool of receptors could be recruited during temporal summation of excitatory synaptic inputs, mediating NMDAR-EPSCs with slow decay kinetics (Zweifel et al., 2009; Drotos et al., 2023). Extrasynaptic NMDARs are most probably recruited during high frequency synaptic activity by glutamate spillover (Lozovaya et al., 2004) when glutamate uptake is limited or overwhelmed (Arnth-Jensen et al., 2002; Asztely et al., 1997) during high regime of synaptic activity. Burst in DA neurons are reminiscent of plateau potentials in layer 5 cortical pyramidal neurons (Oikonomou et al., 2012) or in hippocampal neurons (Suzuki et al., 2008) similarly induced by the activation of extrasynaptic NMDARs via spillover. Extrasynaptic GluN2D-containing NMDARs might favor EPSP-spike coupling, as recently shown for GABAergic neurons (Yao et al., 2022).

Exogenous application of glycine potentiates bursts in SNc DA neurons (Destreel et al., 2019) and enzymatic degradation of the co-agonist decreases burst firing as shown here. Glycine is predominant for the activation of extrasynaptic NMDARs which support bursting. These findings represent mechanistic elements that might be considered for pharmacological treatment of PD. Interestingly, stimulating the activation of NMDARs via its co-agonist site could be beneficial during the late phase of PD (Heresco-Levy et al., 2013). In vivo and clinical investigations showed that administration of sarcosine, a glycine transporter 1 inhibitor, ameliorates some symptoms of PD (Tsai et al., 2014; Frouni et al., 2024). Increasing the amount of glycine might act at extrasynaptic NMDARs and favor bursting activity by SNc DA neurons in patients with PD.

4. Methods

4.1. Experimental model and study participant details

Experiments on Wistar rats were performed in strict accordance with institutional (protocole 2203, Commission d'Éthique Animale, Université de Liège), national (Comité déontologique), and European guidelines for animal experimentation.

5. Method details

5.1. Brain slices preparation

Adolescent 4- to 7-week-old Wistar rats of either sex were anaesthetized with isoflurane (4 % in O_2, Matrx VIP 3000, Midmark) and subsequently killed by decapitation. Before anesthesia animals were kept in an oxygen-enriched chamber for fifteen minutes in order to increase cell survival. Brain slices were prepared as previously described (Destreel et al., 2019). Briefly, after decapitation, the brain was rapidly dissected out and immersed in ice-cold slicing solution containing: 87 mM NaCl, 25 mM $NaHCO_3$, 2.5 mM KCl, 1.25 mM NaH_2PO_4, 10 mM D-glucose, 75 mM sucrose, 0.5 mM $CaCl_2$, and 7 mM $MgCl_2$ (pH 7.4 in 95 % O_2/5 % CO_2, ~325 mOsm). Parasagittal 300 μm-thick (for spontaneous EPSC recordings [sEPSC]) or horizontal 250 μm-thick slices (for electrically evoked EPSCs [eEPSCs]) containing the midbrain were cut using a vibratome (Leica VT-1200, Nussloch, Germany) with a cutting velocity of 0.06 mm/s and a horizontal vibration amplitude of 1.0 mm. Slices containing the SNc were transferred to a storing chamber and allowed to recover at 34°C for 30–45 min. After recovery, slices were kept at room temperature (20 – 25°C) until recording, for up to 4–5 hours.

5.2. Slice electrophysiology

Slices were transferred to a recording chamber and superfused with aCSF containing (in mM): 125 NaCl, 25 $NaHCO_3$, 25 glucose, 2.5 KCl, 1.25 NaH_2PO_4, 2 $CaCl_2$, and 1 $MgCl_2$ (equilibrated with 95 % O_2/5 % CO_2, Osmolarity ~320 mOsm). DA neurons were visualized using infrared-Dodt gradient contrast (IR-DGC) optics and a 40x objective (numerical aperture 0.75, Zeiss, Oberkochen, Germany) on a Zeiss Axio Examiner.A1 microscope equipped with a CCD camera (C7500–51, Hamamatsu, Japan). The location of the medial terminal (MT) nucleus of the accessory optic tract was used as a reference for the SNc area in horizontal slices. DA neurons were identified in whole-cell using current-clamp and voltage-clamp protocols and post hoc using immunohistochemistry. Selected DA neurons had a voltage rectification with hyperpolarizing current steps, action potentials with long half-width, slow autonomous pacemaking (1–4 Hz) and were positive for tyrosine hydroxylase (Fig. S1). Voltage-clamp recordings of DA neurons were conducted with patch pipettes from thick walled borosilicate glass tubing (outer diameter: 2 mm, inner diameter: 1 mm, Hilgenberg, Germany) with a horizontal puller (P-97, Sutter Instruments, Novato, USA). Pipettes were first filled with a potassium gluconate-based internal solution (~1 mm from the tip) and consecutively with a cesium gluconate solution (Wang and Gao, 2010) for whole-cell voltage-clamp recordings. For current-clamp (CC) recordings, pipettes were only filled with a potassium-based solution. The potassium gluconate solution consisted of, in mM: 120 K-gluconate, 20 KCl, 2 $MgCl_2$, 4 Na_2ATP, 0.5 NaGTP, 5 Na_2-phosphocreatine, 0.1 EGTA, 10 HEPES and 0.1 % biocytin (pH = 7.3; osmolarity: ~302 mOsm) and the cesium solution: 120 Cs-gluconate, 20 CsCl, 2 $MgCl_2$, 4 Na_2ATP, 0.5 NaGTP, 5 Na_2-phosphocreatine, 0.1 EGTA, 10 HEPES, 3 QX-314 and 0.1 % biocytin (pH =

7.3; osmolarity: ~306 mOsm). When filled with these solutions, tip resistances were between 3 and 6 MΩ. Voltage- and current-clamp recordings were obtained using a Multiclamp 700B amplifier (Molecular devices, Palo Alto, CA) connected to a PC via a Digidata 1550 interface (Molecular devices). Bridge balance was used to compensate the series resistance (Rs) in current-clamp recordings (R_s <15 MΩ). The current-clamp signal was sampled at 10 kHz. Whole-cell recordings were discarded if the access resistance increased above 15 MΩ for voltage-clamp and above 20 MΩ for current-clamp or if the values varied over 30 % during recording. All voltage-clamp and current-clamp recordings were performed at near-physiological temperature (32–34°C). Bursting activity in SNc DA neurons was generated by bath-applications of NMDA (30 μM) and apamin (300 nM). Hyperpolarizing current injection (from −80 to −140 pA) was applied to maintain membrane potential in a range (~−60 to −80 mV) that facilitated bursting. In these conditions, 100 % of neurons (22 out of 22 neurons) exhibited burst firing (Fig. 1 A, B). To measure time in bursting, the duration of the depolarized plateau at half-height is given for all bursts during a time period of 60 seconds and the value is given in seconds. In the absence of the enzymes, the bursting activity remained stable over 45 minutes (Table S2). Bursting activity in Fig. 5 was recorded using a K^+-based pipette internal solution and TEA and 4-AP in aCSF to block a majority of the potassium conductances in order to stabilize the current baseline at +40 mV in voltage-clamp. TEA and 4-AP were only present in the bath for voltage-clamp recordings and were washed out while switching to current-clamp. In these conditions, bursting could be generated in a majority of DA neurons. Spontaneous EPSCs (sEPSCs) were isolated pharmacologically with picrotoxin (50 μM), CGP 55485 (1 μM) and strychnine (10 μM) to block $GABA_A$, $GABA_B$ and glycine receptor, respectively. Tonic NMDAR-mediated currents were recorded in the presence of CNQX (10 μM), picrotoxin (50 μM), CGP 55485 (1 μM) and strychnine (10 μM). The amplitude of the tonic current was measured by the baseline shift after D-AP5 (50 μM) application.

5.3. Extracellular synaptic stimulation

Afferent fibers were stimulated electrically using theta-glass (borosilicate; Hilgenberg) pipettes (Kumar et al., 2018) filled with a HEPES-buffered sodium-rich solution containing (in mM): 135 NaCl, 5.4 KCl, 1.25 NaH_2PO_4, 1.8 $CaCl_2$, and 1 $MgCl_2$, 5 HEPES (pH adjusted to 7.2 with NaOH). The stimulation pipette was placed rostrally close (within ~100 μm) to the recorded DA neuron and short current pulses were applied (200–600 μA, 200–400 ms) to be slightly above minimal stimulation in order to activate the smallest number of fibers. Excitatory afferent fibers originating from the STN were selected using paired-pulse ratio. Paired-pulse facilitation was used to identify fibers from the STN as reported previously (Beaudoin et al., 2018). Electrically evoked EPSCs (eEPSCs) were isolated pharmacologically with $GABA_A$, $GABA_B$ and glycine receptor blockers (picrotoxin, CGP 55485 and strychnine, respectively). The Zn^{2+} chelator tricine (10 mM) was bath-applied to buffer Zn^{2+} (Vergnano et al., 2014). Ambient zinc (Zn^{2+}) levels exert a tonic inhibition of EPSCs mediated by GluN2A-containing NMDARs due to a high-affinity binding site for Zn^{2+} specifically on this subunit (Paoletti et al., 1997). Zn^{2+} was subsequently added to tricine at a concentration of 60 μM to obtain a concentration of 300 nM free Zn^{2+}. Synaptic NMDARs were selectively blocked by using the irreversible NMDAR antagonist MK-801 (20 μM) applied for 20 min. Electrically evoked EPSCs (eEPSCs) were recorded at a holding potential of V_{hold} = +40 mV under 0.1 Hz stimulation until stable baseline was obtained. Recording configuration was switched to current-clamp with $V_{membrane}$ ~ −80 mV for 20 min during the bath-application of MK-801 and stimulation was stopped. MK-801 was washed out and recording configuration was switched back to voltage-clamp with V_{hold} = +40 mV. Stimulation was resumed and delivered at 5 Hz for 16 s to block selectively synaptic NMDARs (Koh et al., 2022; Liu et al., 2013; Yang et al., 2017). Stimulation < 10 Hz does not induce measurable extrasynaptic NMDAR-mediated current (Harris and Pettit, 2008).

5.4. Immunohistochemistry

Immunohistochemical analysis for identification of DA neurons was done on 300 μm horizontal or parasagittal slices taken after electrophysiological recordings. Biocytin-filled cells were fixed in 4 % paraformaldehyde overnight at 4°C. After washing in phosphate buffer saline (PBS, 0.1 M) and then in PBS containing 10 % normal goat serum (NGS) and 0.3 % triton X-100, slices were incubated with primary antibody against TH (mouse anti-TH 1:1000, Immunostar 22941, Abcam, UK) in PBS containing 5 % goat-serum and 0.3 % Triton X-100 for 22 hours at room temperature. Subsequently, slices were rinsed with PBS and incubated with the secondary antibody (goat-anti-mouse-Alexa Fluor 568 1:500, Invitrogen A-11004, Thermo Fischer Scientitfic, Waltham, MA, USA) together with Fluorescein Avidin DCS (1 μl/ml, Vector Laboratories A-2001–5,) in PBS and 0.3 % triton X-100 overnight at 4°C. After the final rinsing, slices were mounted on a slide containing a 300 μm iSpacer (SunjinLab #IS307, Hsinchu City, Taiwan) with ProLong Gold Antifade (Invitrogen P36934), and imaged using an FV1000 confocal microscope (Olympus, Tokyo, Japan). Images were analyzed with Fiji/ImageJ software (https://imagej.net) and Imaris v9.5.1 (Oxford Instruments, Santa Barbara, CA, USA).

To determine the expression of GluN2 subunits in the SNc immunohistochemical analysis was done on 5- to 6-week-old Wistar rats of either sex. Animals were perfused using a peristaltic pump (Watson Marlow, 101 U) with PBS (150 ml), followed by PBS containing with 4 % PFA (100 ml). Brains were carefully collected, post-fixed in 4 % PFA for 24 hours at 4 °C, subsequently stored in sucrose azide 0.01 % for 48 hours at 4°C and sliced (40 μm) with a NX70 cryostat (Epredia Belgium, Machelen, Belgium). Slices were exposed to 10 % NGS and 0.1 % Triton X-100 followed by primary antibody incubations in PBS containing 5 % NGS and 0.1 % Triton X-100 overnight at 4 °C. Primary antibodies were against GluN2A subunit (rabbit anti-GluN2A 1:200, Alomone AGC-002) combined to mouse anti-TH (1:1000, Immunostar 22941, Abcam, UK), or GluN2B subunit (rabbit anti-GluN2B 1:200, Alomone AGC-003) with mouse anti-TH or GluN2D subunit (rabbit anti-GluN2D 1:200, Alomone AGC-020) with mouse anti-TH in 5 % NGS in PBS and 0.1 % Triton X-100 overnight at 4 °C. After rinsing, slices were incubated with secondary antibodies (goat anti-mouse alexa Fluor 568 1:500, Invitrogen A-11004 and goat anti-rabbit Alexa Fluor 488 1:400, Invitrogen A-11011) in PBS with 0.1 % Triton X-100 for 2 hours at room temperature. Slices were rinsed with PBS and shortly exposed to Dapi (0.5 μg/ml). After mounting with Aqua-poly/mount (Polysciences 18606, Warrington, PA, USA) images were obtained with an FV1000 confocal microscope (Olympus, Tokyo, Japan) using 5x, 40x and 60x oil immersion objectives (N.A. 0.16, 0.8 and 1.4, respectively).

The distribution of the NMDAR subunits within neurons and at their membranes was analyzed with Imaris using videos (Videos S1–S6). Membrane transparency of reconstructed neurons was adjusted by varying the transparency setting implemented in Imaris to differentiate NMDAR subunits expressed in the cytoplasm (100 % transparency - 0 % opacity) from NMDAR subunits in the membrane (0 % transparency - 100 % opacity). TH^+ DA neurons were selected around the MT randomly from both hemispheres.

Supplementary material related to this article can be found online at doi:10.1016/j.pneurobio.2025.102773.

5.5. Enzymes

Recombinant wild-type and M213R variants of *Rhodotorula gracilis* D-amino acid oxidase (RgDAAO; EC 1.4.3.3) and recombinant H244K glycine oxidase from *Bacillus subtilis* (BsGO; EC 1.4.3.19) were produced in *E. coli* cells and purified as previously described (Sacchi et al., 2002; Job et al., 2002; Sonia et al., 2001). The RgDAAO and BsGO preparations had a specific activity of 75 U/mg protein on D-serine as substrate and

2.5 U/mg protein on glycine as substrate, respectively. Midbrain slices were perfused with RgDAAO (0.2 U/ml) or BsGO (0.2 U/ml) for 45 min. For details about RgDAAO and BsGO substrate specificity see (Job et al., 2002; Frattini et al., 2011).

5.6. Drugs and reagents

Picrotoxin (50 μM, Alomone Lab), CGP 55845 hydrochloride (1 μM, Hellobio), strychnine (10 μM, Sigma), TBOA (30 μM, Biotechne) and D-AP5 (50 μM, Alomone labs) were dissolved in doubled distilled water. CNQX disodium (10 μM, Alomone labs) was dissolved in bi-distilled water. Picrotoxin was dissolved in 90 % ethanol. The remaining chemicals and all salts were purchased from Sigma-Aldrich (Belgium).

5.7. High performance liquid chromatography (HPLC) analysis

Slices containing the substantia nigra were stored in the reserve chamber near-physiological temperature (32–34 °C) using three experimental conditions. The first condition was in physiological saline (aCSF), the second in aCSF + GO (0.2 U ml^{-1}) and the third in aCSF + DAAO (0.2 U ml^{-1}) for 45 minutes. The aCSF collected during all experimental conditions were freeze-dried and then resuspended in 25 mM HCl. Following a neutralization step adding 0.2 M NaOH, the samples were precolumn derivatizated with o-phthaldialdehyde/N-acetyl-L-cysteine in a 1:4 volume ratio of 0.2 M borate, pH 8.2, and 0.2 M sodium phosphate, pH 10. Diastereoisomer derivatives were resolved on a Kinetex EVO C18 reverse-phase column (5 μm, 4.6 ×150 mm; Phenomenex, Bologna, MI, Italy) using a HPLC PU-2089 System (Jasco Europe, Cremella, LC, Italy) equipped with a fluorescence detector (344/443 nm, gain 1000X), in isocratic conditions (0.1 M sodium acetate buffer, pH 6.2, 3 % tetrahydrofuran, 0.7 ml/min flow rate), modified from Punzo et al. (2016). Identification and quantification of the D- and L-serine and glycine was based on retention times and peak areas, compared with those associated with external standards (calibration curves were built by injecting 0.005–0.2 pmol of standards). To confirm the identity of D-enantiomers, a selective degradation of D-amino acids in aCSF samples was obtained by adding 10 μg of M213R RgDAAO for 4 h at 30 °C. Statistical analyses were performed using GraphPad Prism 9.0.

6. Quantification and statistical analysis

6.1. Data acquisition and analysis

Pulse generation and data acquisition were performed using clampEx (clampEx 10.5, Molecular Devices). Data analysis was performed using pClamp 10.5 (clampFit), Mathematica 13 (Wolfram Research, Champaign, IL), Stimfit (https://github.com/neurodroid/stimfit/wiki/Stimfit) and Prism 8 (GraphPad software, La Jolla, CA). To detect sEPSCs, MiniAnalysis (v6.0.7, Synaptosoft Inc.) was used and every single event was inspected and selected visually. To obtain an averaged sEPSC, events were superimposed to the initial phase of the current rise. To measure the parameters of the averaged EPSC (amplitude, 20–80 % rise time and decay), a short baseline (5 ms) was used immediately preceding the rise of the event. The averaged event was filtered at 2 kHz. For the analysis of the NMDAR current component of sEPSCs at +40 mV, a dashed vertical line was placed at 10 ms after the onset of the averaged EPSC to evaluate the amplitude of the NMDAR-dependent synaptic current and for eEPSC, it was placed 40 ms after the onset of the event (Li et al., 2013; Jang et al., 2015). At this time point, the AMPAR-current component is back to baseline. The peak amplitude of the AMPAR-current component was measured at the peak of the averaged EPSC at −70 mV. Bursts were defined as spontaneously occurring biphasic changes in the membrane potential during which hyperpolarized periods between −60 and −80 mV alternated with depolarized plateau potentials > −60 mV superimposed by APs. This firing activity was stable and reproducible in the presence of NMDA with the SK channel blocker apamin and hyperpolarizing current injection (Seutin et al., 1993; Destreel et al., 2019).

6.2. Statistical analysis

Experimental values are expressed as mean ± standard error of the mean (SEM). Error bars in the figures also indicate SEM. Statistical analysis was performed using Prism 8. Data were tested for normal distribution with Shapiro-wilk and d'Agostino test. Accordingly, paired-data were either tested by ANOVA 1 test followed by a Tukey post hoc test or Friedman test followed by Dunn's post hoc when more than 2 conditions. Unpaired-data were tested with Kruskal-Wallis test followed by Dunn's test. In the case of 2 conditions, either *t*-test or Wilcoxon test (paired data) and Mann-Withney test (unpaired data) were used. In the case of multiple conditions in 2 different stimulations protocol, ANOVA 2 test followed by a Tukey post hoc test were applied. Significance level is given as $^{*}p < 0.05$, $^{**}p < 0.01$, $^{***}p < 0.001$, $^{****}p < 0.0001$ and ns (not significant) corresponding to $p > 0.05$ is represented in the histograms.

Author contributions

D.E. designed the study. L.P. supplied the enzymes. S.R., L.C. L.V., and Z.M. performed the experiments. S.R. analyzed the data. L.V. helped with anatomy and histology. D.E. supervised the project. D.E. wrote the manuscript. K.J. and V.S. helped to design some experiments.

CRediT authorship contribution statement

Jehasse Kevin: Methodology. **Caldinelli Laura:** Resources, Methodology. **Pollegioni Loredano:** Resources, Methodology, Conceptualization. **Engel Dominique:** Writing – review & editing, Writing – original draft, Supervision, Project administration, Methodology, Funding acquisition, Data curation, Conceptualization. **Ringlet Sofian:** Writing – review & editing, Methodology, Investigation. **Motta Zoraide:** Resources, Methodology, Investigation. **Vandries Laura:** Methodology, Investigation. **Seutin Vincent:** Resources.

Data and code availability

The data described in this paper and any additional information required to reanalyze the data reported in this paper is available from the lead contact upon request.

Declaration of Competing Interest

The authors declare that they have no known competing financial interests or personal relationships that could have appeared to influence the work reported in this paper.

Acknowledgments

We thank Dr. Jean-Marc Goaillard for helpful comments on the manuscript, Sandy El Sayed and Laurent Massotte for technical assistance and the GIGA-imaging platform for using the confocal microscope and Imaris. We also thank particularly Alexandre Hego for his excellent help with analysis using Imaris and Aurore Beuchet for analyzing data. This work was supported by the Belgian FNRS (FRIA), the Fondation Leon Fredericq, Prix de l'espoir from Marie-José De Ridder (to S. R.) and Fonds facultaires de l'ULiège (to D.E). Z.M. is a PhD student of the Life Sciences and Biotechnology course at the University of Insubria. L.P. thanks the support from FAR Fondo di Ateneo per la Ricerca. D.E. thanks Dr. Laurent Nguyen for his support and for integrating D.E. in his (L.N.) Group and Dr. Sophie Laguesse for sharing data.

Appendix A. Supporting information

Supplementary data associated with this article can be found in the online version at doi:10.1016/j.pneurobio.2025.102773.

Data availability

Data will be made available on request.

References

Ammari, R., Lopez, C., Fiorentino, H., Gonon, F., Hammond, C., 2009. A mouse juvenile or adult slice with preserved functional nigro-striatal dopaminergic neurons. Neuroscience 159, 3–6. https://doi.org/10.1016/j.neuroscience.2008.10.051.

Arnth-Jensen, N., Jabaudon, D., Scanziani, M., 2002. Cooperation between independent hippocampal synapses is controlled by glutamate uptake. Nat. Neurosci. 5, 325–331. https://doi.org/10.1038/nn825.

Asztely, F., Erdemli, G., Kullmann, D.M., 1997. Extrasynaptic glutamate spillover in the hippocampus: dependence on temperature and the role of active glutamate uptake. Neuron 18, 281–293. https://doi.org/10.1016/S0896-6273(00)80268-8.

Balsara, R.D., Ferreira, A.N., Donahue, D.L., Castellino, F.J., Sheets, P.L., 2014. Probing NMDA receptor GluN2A and GluN2B subunit expression and distribution in cortical neurons. Neuropharmacology 79, 542–549. https://doi.org/10.1016/j.neuropharm.2014.01.005.

Beaudoin, G., Gomez, J., Perkins, J., Bland, J., Petko, A., Paladini, C., 2018. Cocaine selectively reorganizes excitatory inputs to substantia Nigra pars compacta dopamine neurons. J. Neurosci. 38, 1151–1159. https://doi.org/10.1523/JNEUROSCI.1975-17.2017.

Berger, A.J., Dieudonné, S., Ascher, P., 1998. Glycine uptake governs glycine site occupancy at NMDA receptors of excitatory synapses. J. Neurophysiol. 80, 3336–3340. https://doi.org/10.1152/jn.1998.80.6.3336.

Blythe, S.N., Atherton, J.F., Bevan, M.D., 2007. Synaptic activation of dendritic AMPA and NMDA receptors generates transient high-frequency firing in substantia nigra dopamine neurons in vitro. J. Neurophysiol. 97, 2837–2850. https://doi.org/10.1152/jn.01157.2006.

Brickley, S.G., Misra, C., Mok, M.H.S., Mishina, M., Cull-Candy, S.G., 2003. NR2B and NR2D subunits coassemble in cerebellar golgi cells to form a distinct NMDA receptor subtype restricted to extrasynaptic sites. J. Neurosci. 23, 4958–4966. https://doi.org/10.1523/JNEUROSCI.23-12-04958.2003.

Brothwell, S.L.C., Barber, J.L., Monaghan, D.T., Jane, D.E., Gibb, A.J., Jones, S., 2008. NR2B- and NR2D-containing synaptic NMDA receptors in developing rat substantia nigra pars compacta dopaminergic neurones. J. Physiol. 586, 739–750. https://doi.org/10.1113/jphysiol.2007.144618.

Chergui, K., Charléty, P.J., Akaoka, H., Saunier, C.F., Brunet, J. -L., Buda, M., Svensson, T.H., Chouvet, G., 1993. Tonic activation of NMDA receptors causes spontaneous burst discharge of rat midbrain dopamine neurons in vivo. Eur. J. Neurosci. 5, 137–144. https://doi.org/10.1111/j.1460-9568.1993.tb00479.x.

Chergui, K., Akaoka, H., Charléty, P.J., Saunier, C.F., Buda, M., Chouvet, G., 1994. Subthalamic nucleus modulates burst firing of nigral dopamine neurones via NMDA receptors. Neuroreport 5, 1185–1188. https://doi.org/10.1097/00001756-199406020-00006.

Cubelos, B., Giménez, C., Zafra, F., 2005. Localization of the GLYT1 glycine transporter at glutamatergic synapses in the rat brain. Cereb. Cortex 15, 448–459. https://doi.org/10.1093/cercor/bhh147.

Curcio, L., Podda, M.V., Leone, L., Piacentini, R., Mastrodonato, A., Cappelletti, P., Sacchi, S., Pollegioni, L., Grassi, C., D'Ascenzo, M., 2013. Reduced D-serine levels in the nucleus accumbens of cocaine-treated rats hinder the induction of NMDA receptor-dependent synaptic plasticity. Brain 136, 1216–1230. https://doi.org/10.1093/brain/awt036.

Currás, M.C., Pallotta, B.S., 1996. Single-channel evidence for glycine and NMDA requirement in NMDA receptor activation. Brain Res 740, 27–40. https://doi.org/10.1016/S0006-8993(96)00845-1.

Destreel, G., Seutin, V., Engel, D., 2019. Subsaturation of the N-methyl-D-aspartate receptor glycine site allows the regulation of bursting activity in juvenile rat nigral dopamine neurons. Eur. J. Neurosci. 50, 3454–3471. https://doi.org/10.1111/ejn.14491.

Dopico, J.G., González-Hernández, T., Pérez, I.M., García, I.G., Abril, A.M., Inchausti, J. O., Rodríguez Díaz, M., 2006. Glycine release in the substantia nigra: interaction with glutamate and GABA. Neuropharmacology 50, 548–557. https://doi.org/10.1016/j.neuropharm.2005.10.014.

Drotos, A.C., Zarb, R.L., Booth, V., and Roberts, M.T. (2023). GluN2C/D-containing NMDA receptors enhance temporal summation and increase sound-evoked and spontaneous firing in the inferior colliculus. bioRxiv preprint. https://doi.org/10.1101/2023.04.27.538607.

Ferreira, J.S., Papouin, T., Ladépêche, L., Yao, A., Langlais, V.C., Bouchet, D., Dulong, J., Mothet, J.P., Sacchi, S., Pollegioni, L., et al., 2017. Co-agonists differentially tune GluN2B-NMDA receptor trafficking at hippocampal synapses. Elife 6, 1–22. https://doi.org/10.7554/eLife.25492.

Fossat, P., Turpin, F.R., Sacchi, S., Dulong, J., Shi, T., Rivet, J.M., Sweedler, J.V., Pollegioni, L., Millan, M.J., Oliet, S.H.R., et al., 2012. Glial D-serine gates NMDA receptors at excitatory synapses in prefrontal cortex. Cereb. Cortex 22, 595–606. https://doi.org/10.1093/cercor/bhr130.

Frattini, L., Rosini, E., Pollegioni, L., Pilone, M.S., 2011. Analyzing the d-amino acid content in biological samples by engineered enzymes. J. Chromatogr. B 879, 3235–3239. https://doi.org/10.1016/j.jchromb.2011.02.036.

Frouni, I., Kim, E., Shaqfah, J., Bédard, D., Kwan, C., Belliveau, S., Huot, P., 2024. [3H]-NFPS binding to the glycine transporter 1 in the hemi-parkinsonian rat brain. Exp. Brain Res 242, 1203–1214. https://doi.org/10.1007/s00221-024-06815-w.

Gibb, A.J., 2022. Allosteric antagonist action at triheteromeric NMDA receptors. Neuropharmacology 202, 1–7. https://doi.org/10.1016/j.neuropharm.2021.108861.

Gonon, F.G., 1988. Nonlinear relationship between impulse flow and dopamine released by rat midbrain dopaminergic neurons as studied by in vivo electrochemistry. Neuroscience 24, 19–28. https://doi.org/10.1016/0306-4522(88)90307-7.

Grace, A.A., Bunney, B.S., 1984. The control of firing pattern in nigral dopamine neurons: burst firing. J. Neurosci. 4, 2877–2890. https://doi.org/10.1523/JNEUROSCI.04-11-02877.1984.

Hage, T.A., Khaliq, Z.M., 2015. Tonic firing rate controls dendritic Ca2+ signaling and synaptic gain in substantia nigra dopamine neurons. J. Neurosci. 35, 5823–5836. https://doi.org/10.1523/JNEUROSCI.3904-14.2015.

Hansen, K.B., Wollmuth, L.P., Bowie, D., Furukawa, H., Menniti, F.S., Sobolevsky, A.I., Swanson, G.T., Swanger, S.A., Greger, I.H., Nakagawa, T., et al., 2021. Structure, function, and pharmacology of glutamate receptor ion channels. Pharm. Rev. 73, 1469–1658. https://doi.org/10.1124/pharmrev.120.000131.

Hardingham, G.E., Bading, H., 2010. Synaptic versus extrasynaptic NMDA receptor signalling: implications for neurodegenerative disorders. Nat. Rev. Neurosci. 11, 682–696. https://doi.org/10.1038/nrn2911.

Harnett, M.T., Bernier, B.E., Ahn, K.-C., Morikawa, H., 2009. Burst-timing-dependent plasticity of NMDA receptor-mediated transmission in midbrain dopamine neurons. Neuron 62, 826–838. https://doi.org/10.1016/j.neuron.2009.05.011.

Harney, S.C., Jane, D.E., Anwyl, R., 2008. Extrasynaptic NR2D-containing NMDARs are recruited to the synapse during LTP of NMDAR-EPSCs. J. Neurosci. 28, 11685–11694. https://doi.org/10.1523/JNEUROSCI.3035-08.2008.

Harris, A.Z., Pettit, D.L., 2007. Extrasynaptic and synaptic NMDA receptors form stable and uniform pools in rat hippocampal slices. J. Physiol. 584, 509–519. https://doi.org/10.1113/jphysiol.2007.137679.

Harris, A.Z., Pettit, D.L., 2008. Recruiting extrasynaptic NMDA receptors augments synaptic signaling. J. Neurophysiol. 99, 524–533. https://doi.org/10.1152/jn.01169.2007.

Heresco-Levy, U., Shoham, S., Javitt, D.C., 2013. Glycine site agonists of the N-methyl-d-aspartate receptor and Parkinson's disease: a hypothesis. Mov. Disord. 28, 419–424. https://doi.org/10.1002/mds.25306.

Hornykiewicz, O., 2006. The discovery of dopamine deficiency in the parkinsonian brain. Parkinson's Disease and Related Disorders. Springer Vienna, pp. 9–15. https://doi.org/10.1007/978-3-211-45295-0_3.

Howe, M.W., Dombeck, D.A., 2016. Rapid signalling in distinct dopaminergic axons during locomotion and reward. Nature 535, 505–510. https://doi.org/10.1038/nature18942.

Huettner, J.E., Bean, B.P., 1988. Block of N-methyl-D-aspartate-activated current by the anticonvulsant MK-801: selective binding to open channels. Proc. Natl. Acad. Sci. 85, 1307–1311. https://doi.org/10.1073/pnas.85.4.1307.

Jang, M., Um, K.B., Jang, J., Kim, H.J., Cho, H., Chung, S., Park, M.K., 2015. Coexistence of glutamatergic spine synapses and shaft synapses in substantia nigra dopamine neurons. Sci. Rep. 5, 14773. https://doi.org/10.1038/srep14773.

Job, V., Molla, G., Pilone, M.S., Pollegioni, L., 2002. Overexpression of a recombinant wild-type and His-tagged *Bacillus subtilis* glycine oxidase in *Escherichia coli*. Eur. J. Biochem 269, 1456–1463. https://doi.org/10.1046/j.1432-1033.2002.02790.x.

Johnson, J.W., and Ascher, P. (1987). Glycine potentiates the NMDA response in cultured mouse brain neurons. Preprint, https://doi.org/10.1038/325529a0 https://doi.org/10.1038/325529a0.

Jones, S., Gibb, A.J., 2005. Functional NR2B- and NR2D-containing NMDA receptor channels in rat substantia nigra dopaminergic neurones. J. Physiol. 569, 209–221. https://doi.org/10.1113/jphysiol.2005.095554.

Kleckner, N.W., Dingledine, R., 1988. Requirement for glycine in activation of NMDA-receptors expressed in xenopus oocytes. Science 241, 835–837. https://doi.org/10.1126/science.2841759.

Koh, W., Park, M., Chun, Y.E., Lee, J., Shim, H.S., Park, M.G., Kim, S., Sa, M., Joo, J., Kang, H., et al., 2022. Astrocytes render memory flexible by releasing D-serine and regulating NMDA receptor tone in the hippocampus. Biol. Psychiatry 91, 740–752. https://doi.org/10.1016/j.biopsych.2021.10.012.

Kumar, A., Schiff, O., Barkai, E., Mel, B.W., Poleg-Polsky, A., Schiller, J., 2018. NMDA spikes mediate amplification of inputs in the rat piriform cortex. Elife 7. https://doi.org/10.7554/eLife.38446.

Le Bail, M., Martineau, M., Sacchi, S., Yatsenko, N., Radzishevsky, I., Conrod, S., Ait Ouares, K., Wolosker, H., Pollegioni, L., Billard, J.-M., et al., 2015. Identity of the NMDA receptor coagonist is synapse specific and developmentally regulated in the hippocampus. Proc. Natl. Acad. Sci. USA 112, E204–E213. https://doi.org/10.1073/pnas.1416668112.

Le Meur, K., Galante, M., Angulo, M.C., Audinat, E., 2007. Tonic activation of NMDA receptors by ambient glutamate of non-synaptic origin in the rat hippocampus. J. Physiol. 580, 373–383. https://doi.org/10.1113/jphysiol.2006.123570.

Li, Y., Sacchi, S., Pollegioni, L., Basu, A.C., Coyle, J.T., Bolshakov, V.Y., 2013. Identity of endogenous NMDAR glycine site agonist in amygdala is determined by synaptic activity level. Nat. Commun. 4, 1760. https://doi.org/10.1038/ncomms2779.

Liu, D., Yang, Q., Li, S., 2013. Activation of extrasynaptic NMDA receptors induces LTD in rat hippocampal CA1 neurons. Brain Res Bull. 93, 10–16. https://doi.org/10.1016/j.brainresbull.2012.12.003.

Lozovaya, N.A., Grebenyuk, S.E., Tsintsadze, T.Sh, Feng, B., Monaghan, D.T., Krishtal, O. A., 2004. Extrasynaptic NR2B and NR2D subunits of NMDA receptors shape 'superslow' afterburst EPSC in rat hippocampus. J. Physiol. 558, 451–463. https://doi.org/10.1113/jphysiol.2004.063792.

Momiyama, A., 2000. Distinct synaptic and extrasynaptic NMDA receptors identified in dorsal horn neurones of the adult rat spinal cord. J. Physiol. 523, 621–628. https://doi.org/10.1111/j.1469-7793.2000.t01-1-00621.x.

Morabito, A., Zerlaut, Y., Serraz, B., Sala, R., Paoletti, P., Rebola, N., 2022. Activity-dependent modulation of NMDA receptors by endogenous zinc shapes dendritic function in cortical neurons. Cell Rep. 38, 110415. https://doi.org/10.1016/j.celrep.2022.110415.

Nozaki, C., Vergnano, A.M., Filliol, D., Ouagazzal, A.-M., Le Goff, A., Carvalho, S., Reiss, D., Gaveriaux-Ruff, C., Neyton, J., Paoletti, P., et al., 2011. Zinc alleviates pain through high-affinity binding to the NMDA receptor NR2A subunit. Nat. Neurosci. 14, 1017–1022. https://doi.org/10.1038/nn.2844.

Oikonomou, K.D., Short, S.M., Rich, M.T., Antic, S.D., 2012. Extrasynaptic glutamate receptor activation as cellular bases for dynamic range compression in pyramidal neurons. Front Physiol. 1–22. https://doi.org/10.3389/fphys.2012.00334.

Otomo, K., Perkins, J., Kulkarni, A., Stojanovic, S., Roeper, J., Paladini, C.A., 2020. In vivo patch-clamp recordings reveal distinct subthreshold signatures and threshold dynamics of midbrain dopamine neurons. Nat. Commun. 11, 1–15. https://doi.org/10.1038/s41467-020-20041-2.

Panatier, A., Theodosis, D.T., Mothet, J.P., Touquet, B., Pollegioni, L., Poulain, D.A., Oliet, S.H.R., 2006. Glia-derived D-serine controls NMDA receptor activity and synaptic memory. Cell 125, 775–784. https://doi.org/10.1016/j.cell.2006.02.051.

Paoletti, P., Ascher, P., Neyton, J., 1997. High-affinity zinc inhibition of NMDA NR1–NR2A receptors. J. Neurosci. 17, 5711–5725. https://doi.org/10.1523/JNEUROSCI.17-15-05711.1997.

Paoletti, P., Vergnano, A.M., Barbour, B., Casado, M., 2009. Zinc at glutamatergic synapses. Neuroscience 158, 126–136. https://doi.org/10.1016/j.neuroscience.2008.01.061.

Papouin, T., Ladépêche, L., Ruel, J., Sacchi, S., Labasque, M., Hanini, M., Groc, L., Pollegioni, L., Mothet, J.P., Oliet, S.H.R., 2012. Synaptic and extrasynaptic NMDA receptors are gated by different endogenous coagonists. Cell 150, 633–646. https://doi.org/10.1016/j.cell.2012.06.029.

Perszyk, R.E., DiRaddo, J.O., Strong, K.L., Low, C.M., Ogden, K.K., Khatri, A., Vargish, G. A., Pelkey, K.A., Tricoire, L., Liotta, D.C., et al., 2016. GluN2D-containing N-methyl-D-aspartate receptors mediate synaptic transmission in hippocampal interneurons and regulate interneuron activity. Mol. Pharm. 90, 689–702. https://doi.org/10.1124/mol.116.105130.

Petralia, R.S., Wang, Y.X., Hua, F., Yi, Z., Zhou, A., Ge, L., Stephenson, F.A., Wenthold, R. J., 2010. Organization of NMDA receptors at extrasynaptic locations. Neuroscience 167, 68–87. https://doi.org/10.1016/j.neuroscience.2010.01.022.

Punzo, D., Errico, F., Cristino, L., Sacchi, S., Keller, S., Belardo, C., Luongo, L., Nuzzo, T., Imperatore, R., Florio, E., et al., 2016. Age-related changes in d-aspartate oxidase promoter methylation control extracellular d-aspartate levels and prevent precocious cell death during brain aging. J. Neurosci. 36, 3064–3078. https://doi.org/10.1523/JNEUROSCI.3881-15.2016.

Rauner, C., Köhr, G., 2011. Triheteromeric NR1/NR2A/NR2B receptors constitute the major N-methyl-D-aspartate receptor population in adult hippocampal synapses. J. Biol. Chem. 286, 7558–7566. https://doi.org/10.1074/jbc.M110.182600.

Riebe, I., Seth, H., Culley, G., Dósa, Z., Radi, S., Strand, K., Fröjd, V., Hanse, E., 2016. Tonically active NMDA receptors - a signalling mechanism critical for interneuronal excitability in the CA1 stratum radiatum. Eur. J. Neurosci. 43, 169–178. https://doi.org/10.1111/ejn.13128.

Sacchi, S., Lorenzi, S., Molla, G., Pilone, M.S., Rossetti, C., Pollegioni, L., 2002. Engineering the substrate specificity ofd-amino-acid oxidase. J. Biol. Chem. 277, 27510–27516. https://doi.org/10.1074/jbc.M203946200.

Seutin, V., Johnson, S.W., North, R.A., 1993. Apamin increases NMDA-induced burst-firing of rat mesencephalic dopamine neurons. Brain Res. 630, 341–344. https://doi.org/10.1016/0006-8993(93)90675-D.

da Silva, J.A., Tecuapetla, F., Paixão, V., Costa, R.M., 2018. Dopamine neuron activity before action initiation gates and invigorates future movements. Nature 554, 244–248. https://doi.org/10.1038/nature25457.

Soden, M.E., Jones, G.L., Sanford, C.A., Chung, A.S., Güler, A.D., Chavkin, C., Luján, R., Zweifel, L.S., 2013. Disruption of dopamine neuron activity pattern regulation through selective expression of a human KCNN3 mutation. Neuron 80, 997–1009. https://doi.org/10.1016/j.neuron.2013.07.044.

Sonia, F., Loredano, P., Mirella, P.S., 2001. Engineering, expression and purification of a His-tagged chimeric D-amino acid oxidase from Rhodotorula gracilis. Enzym. Micro Technol. 29, 407–412. https://doi.org/10.1016/S0141-0229(01)00400-8.

Stroebel, D., Casado, M., Paoletti, P., 2018. Triheteromeric NMDA receptors: from structure to synaptic physiology. Curr. Opin. Physiol. 2, 1–12. https://doi.org/10.1016/j.cophys.2017.12.004.

Suzuki, T., Kodama, S., Hoshino, C., Izumi, T., Miyakawa, H., 2008. A plateau potential mediated by the activation of extrasynaptic NMDA receptors in rat hippocampal CA1 pyramidal neurons. Eur. J. Neurosci. 28, 521–534. https://doi.org/10.1111/j.1460-9568.2008.06324.x.

Swanger, S.A., Vance, K.M., Pare, J.F., Sotty, F., Fog, K., Smith, Y., Traynelis, S.F., 2015. NMDA receptors containing the GluN2D subunit control neuronal function in the subthalamic nucleus. J. Neurosci. 35, 15971–15983. https://doi.org/10.1523/JNEUROSCI.1702-15.2015.

Tsai, C.H., Huang, H.C., Liu, B.L., Li, C.I., Lu, M.K., Chen, X., Tsai, M.C., Yang, Y.W., Lane, H.Y., 2014. Activation of N-methyl-D-aspartate receptor glycine site temporally ameliorates neuropsychiatric symptoms of Parkinson's disease with dementia. Psychiatry Clin. Neurosci. 68, 692–700. https://doi.org/10.1111/pcn.12175.

Vergnano, A.M., Rebola, N., Savtchenko, L.P., Pinheiro, P.S., Casado, M., Kieffer, B.L., Rusakov, D.A., Mulle, C., Paoletti, P., 2014. Zinc dynamics and action at excitatory synapses. Neuron 82, 1101–1114. https://doi.org/10.1016/j.neuron.2014.04.034.

Wang, H., Gao, W., 2010. Development of calcium-permeable AMPA receptors and their correlation with NMDA receptors in fast-spiking interneurons of rat prefrontal cortex. J. Physiol. 588, 2823–2838. https://doi.org/10.1113/jphysiol.2010.187591.

Wang, H., Stradtman, G.G., Wang, X.-J., Gao, W.-J., 2008. A specialized NMDA receptor function in layer 5 recurrent microcircuitry of the adult rat prefrontal cortex. Proc. Natl. Acad. Sci. 105, 16791–16796. https://doi.org/10.1073/pnas.0804318105.

Wang, L.P., Li, F., Wang, D., Xie, K., Wang, D., Shen, X., Tsien, J.Z., 2011. NMDA receptors in dopaminergic neurons are crucial for habit learning. Neuron 72, 1055–1066. https://doi.org/10.1016/j.neuron.2011.10.019.

Watabe-Uchida, M., Zhu, L., Ogawa, S.K., Vamanrao, A., Uchida, N., 2012. Whole-brain mapping of direct inputs to midbrain dopamine neurons. Neuron 74, 858–873. https://doi.org/10.1016/j.neuron.2012.03.017.

Wild, A.R., Bollands, M., Morris, P.G., Jones, S., 2015. Mechanisms regulating spill-over of synaptic glutamate to extrasynaptic NMDA receptors in mouse substantia nigra dopaminergic neurons. Eur. J. Neurosci. 42, 2633–2643. https://doi.org/10.1111/ejn.13075.

Yang, Q., Zhu, G., Liu, D., Ju, J.G., Liao, Z.H., Xiao, Y.X., Zhang, Y., Chao, N., Wang, J., Li, W., et al., 2017. Extrasynaptic NMDA receptor dependent long-term potentiation of hippocampal CA1 pyramidal neurons. Sci. Rep. 7, 1–9. https://doi.org/10.1038/s41598-017-03287-7.

Yao, L., Rong, Y., Ma, X., Li, H., Deng, D., Chen, Y., Yang, S., Peng, T., Ye, T., Liang, F., et al., 2022. Extrasynaptic NMDA receptors bidirectionally modulate intrinsic excitability of inhibitory neurons. J. Neurosci. 42, 3066–3079. https://doi.org/10.1523/JNEUROSCI.2065-21.2022.

Yi, F., Bhattacharya, S., Thompson, C.M., Traynelis, S.F., Hansen, K.B., 2019. Functional and pharmacological properties of triheteromeric GluN1/2B/2D NMDA receptors. J. Physiol. 597, 5495–5514. https://doi.org/10.1113/JP278168.

Zweifel, L.S., Parker, J.G., Lobb, C.J., Rainwater, A., Wall, V.Z., Fadok, J.P., Darvas, M., Kim, M.J., Mizumori, S.J., Paladini, C.A., et al., 2009. Disruption of NMDAR-dependent burst firing by dopamine neurons provides selective assessment of phasic dopamine-dependent behavior. Proc. Natl. Acad. Sci. USA 106, 7281–7288. https://doi.org/10.1073/pnas.0813415106.